A Global Climatology of Extratropical Transition

Melanie Bieli*

Department of Applied Physics and Applied Mathematics, Columbia University, New York, NY

Suzana J. Camargo

Lamont-Doherty Earth Observatory, Columbia University, Palisades, NY

Adam H. Sobel

Department of Applied Physics and Applied Mathematics, Columbia University, New York, NY, and Lamont-Doherty Earth Observatory, Columbia University, Palisades, NY

Jenni L. Evans

Department of Meteorology and Atmospheric Science, Pennsylvania State University, University Park, PA

Timothy Hall

NASA Goddard Institute for Space Studies, New York, NY

Corresponding author address: Melanie Bieli, Department of Applied Physics and Applied Mathematics, Columbia University, New York, NY

E-mail: mb4036@columbia.edu

ABSTRACT

The authors diagnose tropical cyclones that undergo extratropical transition (ET) in the cyclone phase space (CPS) on a global basis. Best-track data from 1979-2015 are used to define the tracks of the storms, and geopotential height fields from reanalysis datasets are used to locate each storm in the CPS. Two reanalyses are employed and compared for this purpose, the Japanese 55-year Reanalysis (JRA-55) and the ECMWF Interim Reanalysis (ERA-Interim). The results are used to study the seasonal and geographical distributions of storms undergoing ET, inter-basin differences in the statistics of ET occurrence, and the differences between the ETs defined by CPS and those defined by the 'extratropical' labels (determined subjectively by human forecasters) in the best-track archives. About 50% of all storms in the North Atlantic and the Western North Pacific undergo ET. In the southern hemisphere, ET fractions range from about 20% in the South Indian Ocean and the Australian region to 40% in the South Pacific. The North Atlantic and Western North Pacific exhibit somewhat different seasonal cycles, with the probability of ET maximizing later in the North Atlantic, but having a local minimum in the earlier part of the peak season in both basins. The classification of ET storms based on JRA-55 agrees better with the best-track data than does the ERA-Interim classification. In the North Atlantic and the Western North Pacific, the differences are small and both reanalyses achieve F1 performance scores of at least 0.8, but JRA-55 has a higher classification skill in all other basins.

1. Introduction

Towards the end of their lifetimes, tropical cyclones (TCs) often undergo a process called extratropical transition (ET), in which they radically change their physical structure and develop characteristics typical of extratropical cyclones. ET occurs as a TC moves into higher latitudes and encounters cooler sea surface temperatures and stronger vertical wind shear (Jones et al. 2003). The baroclinic environment sets the stage for the transition of the TC: As colder, drier air intrudes into the warm core, the storm loses its radial symmetry and begins to tilt toward the cold upper-level air. Eventually the TC becomes a cold-core system with asymmetric, frontal structure, completing its transition to an extratropical cyclone.

During ET, a storm may reintensify as it starts to tap baroclinic energy in addition to the energy source residing in the thermodynamic disequilibrium between the atmosphere and the underlying ocean. Often the system also accelerates its forward motion and produces intense precipitation, strong winds and large surface water waves, posing a serious threat to coastal regions and maritime activities (Jones et al. 2003). In particular, tropical systems that reintensify after ET in the North Atlantic can constitute a hazard for Canada and/or northwest Europe – e.g., the transitioning Hurricane Igor (2010) caused severe flooding in Newfoundland (Masson 2014), and the extratropical system that developed from Hurricane Lili (1996) was responsible for seven deaths and substantial economic losses in Europe (Agustí-Panareda et al. 2005).

However, not all TCs rejuvenate and strengthen during ET – some decay, while others don't undergo transition at all, even when moving poleward into baroclinic regions. The extratropical fate of a TC is difficult to forecast – in general, the "rebirth" of a TC as an extratropical cyclone is more likely to happen over ocean and when an upper-level trough approaching from the west connects with the tropical system (Emanuel 2005; Hart and Evans 2001; Matano and Sekioka

1971). This interaction may not only transform the storm, but also alter the large-scale midlatitude flow, causing poor synoptic predictability over a wide area downstream (e.g., Anwender et al. 2008; Keller 2012, 2017).

Around the turn of the millennium, the increasing awareness that the nature of a storm can change over the course of its life cycle sparked research on case studies of individual transitions (e.g., Atallah and Bosart 2003; McTaggart-Cowan et al. 2003; Thorncroft and Jones 2000) as well as on basin-specific climatologies (e.g., Klein et al. 2000; Hart and Evans 2001; Sinclair 2002). However, advances in research were hindered by the lack of an objective definition of ET. This gap was filled by the cyclone phase space (CPS) framework proposed by Hart (2003), which has since become well-established and widely used.

The CPS allows for automated and objective detection of ET in large sets of storms and hence paved the way for statistical approaches to describe the phenomenon. This motivated more recent ET climatologies in various ocean basins (e.g., Kitabatake 2011; Wood and Ritchie 2014). However, these studies mostly focus on single ocean basins and use a variety of data sets. Moreover, they include different modifications to the original CPS-based definition of ET in Hart (2003), which makes their results difficult to compare.

This lack of a global perspective on ET provides the first part of the motivation for the study at hand: Using a consistent set of data, time period, and method, we present a global CPS-based climatology of ET that encompasses all major cyclone basins.

The second aim of this study is then to examine how well the CPS-based ET detection agrees with the ET cases diagnosed by forecasters, for individual storms as well as in terms of statistical performance measures. This second part of the study is particularly important for the application of the CPS in global climate models (Zarzycki et al. 2016; Liu et al. 2017), which are growing more realistic in their representation of TCs and where an ET climatology based on a globally consistent

methodology is fundamental to determine the model performance in the current climate, as well as the uncertainty in future projections of ET. Thus, the present study lays the foundation for future work assessing how a warming climate could potentially impact transitioning TCs.

2. Data and Methods

a. TC Best-Track and Reanalysis Datasets

The two basic ingredients for the analysis presented here are global TC track data and geopotential height fields from reanalysis datasets. Here we consider best-track datasets from the National Hurricane Center (NHC) in the North Atlantic (NAT) and in the Eastern and Central North Pacific (ENP), from the Joint Typhoon Warning Center (JTWC) in the North Indian Ocean (NI), the Southern Hemisphere (SH), and the Western North Pacific (WNP), and from the Japan Meteorological Agency (JMA) in the WNP. Within the SH, we distinguish the South Indian Ocean (SI), the Australian region (AUS), and the South Pacific (SP).

The best-track data provide information on the position of the storm center, maximum wind speed, and the type of the storm as declared by the respective operational meteorological agencies. In the best-track archives of the JTWC, the 'storm type' records only start in 2003. For our analysis, we consider TCs that occurred in the satellite era 1979-2015 and exclude storms that never developed wind speeds greater than 33 kt, i.e., that remained at or below tropical depression intensity throughout their lifetimes. Table 1 highlights the key characteristics of the resulting set of storms and complements Fig. 1, which shows a subset of the storm tracks examined in this study, together with the boundaries of the ocean basins.

In order to examine the sensitivity of the results with respect to the reanalysis dataset considered, all calculations were performed on the Japanese 55-year Reanalysis (JRA-55; $1.25^\circ \times 1.25^\circ$)

released by the JMA (Kobayashi et al. 2015) as well as on the European Centre for Medium-Range Weather Forecasts' (ECMWF) Interim Reanalysis (ERA-Interim; $0.7^\circ \times 0.7^\circ$; Dee et al. 2011). Both datasets are considered state-of-the-art reanalyses and apply a four-dimensional variational data assimilation to provide dynamically consistent estimates of the state of the atmosphere in 6-hourly time steps. It is worth noting that the JRA-55 assimilation system uses artificial wind profile retrievals in the vicinity of TCs. Generated by synthetic dropwindsondes, they approximate the TC wind profile at the best-track locations and are then processed like observed data (Ebita et al. 2011). ERA-Interim, on the other hand, does not assimilate any artificial TC information.

Schenkel and Hart (2012) found that there can be considerable position and intensity differences between the best-track TCs and the corresponding TCs in the reanalysis, especially for weak storms in observation-scarce regions. To gauge the effect of these possible mismatches, the best-track positions were mapped to the closest JRA-55 sea-level pressure minimum within a 300-km radius. However, the results derived from these recentered tracks barely differed from those of the original tracks, therefore we don't include them here.

b. Cyclone Phase Space (CPS)

We employ the CPS proposed by Hart (2003) to objectively identify storms that undergo ET. In the CPS framework, the physical structure of cyclones is described based on three parameters that can all be computed from geopotential height fields: The B parameter measures the asymmetry in the geopotential thickness surrounding the cyclone, and two thermal wind (V_T) parameters assess whether the cyclone has a warm or cold core structure in the upper (V_T^U) and lower (V_T^L) troposphere.

The B parameter is computed by taking the difference between the average 900-600-hPa geopotential thickness to the right and to the left of the storm, in a radius of 500 km around the storm

center:

$$B = h\left(\overline{Z_{600\text{ hPa}} - Z_{900\text{ hPa}}}\Big|_{\text{R}} - \overline{Z_{600\text{ hPa}} - Z_{900\text{ hPa}}}\Big|_{\text{L}}\right),$$

where Z is geopotential height, R indicates right relative to the storm motion, L indicates left of the storm, and the overbar indicates the areal mean over a semicircle of radius 500 km. The hemispheric parameter h is 1 for the northern hemisphere and -1 for the southern hemisphere. Thermally symmetric storms will thus have B values close to zero, while large B values represent thermally asymmetric storms.

The parameters V_T^L and V_T^U evaluate the thermal wind in the 900-600 hPa layer and the 600-300 hPa layer, respectively:

$$-V_T^L = \frac{\partial \Delta Z}{\partial(\ln p)}\Bigg|_{900\text{ hPa}}^{600\text{ hPa}}$$
$$-V_T^U = \frac{\partial \Delta Z}{\partial(\ln p)}\Bigg|_{600\text{ hPa}}^{300\text{ hPa}}$$

They are computed by linear regression of the difference in maximum and minimum geopotential height between isobaric levels, again within a radius of 500 km. Positive values of $-V_T^L$ and $-V_T^U$ (weakening geostrophic wind with height) then indicate the presence of a warm (tropical) core in that layer, while strengthening winds with height lead to negative values and are associated with cold-cored (extratropical) systems.

In summary, TCs are characterized by small values of B and positive values of $-V_T^L$ and $-V_T^U$, while extratropical storms have large values of B and negative values of $-V_T^L$ and $-V_T^U$. As described by Hart (2003), transitioning storms typically follow a trajectory where the storm first loses its symmetry before developing a cold core in the lower troposphere. Evans and Hart (2003) then define the onset of ET as the time when the B parameter first exceeds a value of 10, while the subsequent drop of $-V_T^L$ below zero marks the end of the process.

For this study, the original definition has been modified with the purpose of maximizing the agreement with the ET cases in the best-track datasets: We increased the B threshold to 11 and required $-V_T^U$ (not just $-V_T^L$) to become negative for a successful ET completion, i.e., we required the cyclone to develop a cold-core structure throughout the 900-300 hPa layer. Evans and Hart (2003) argued that as the upper troposphere usually becomes cold prior to the lower troposphere, thermal wind in the lower troposphere provides a more stringent criterion on transition completion than the upper-tropospheric thermal wind, and hence they did not impose any condition on $-V_T^U$. The inclusion of the $-V_T^U$ criterion is further discussed in section 3.b.1. In addition, ET onset was only declared if a storm had wind speeds of at least 33 kt, as some tropical depression-like systems or monsoonal troughs raise false alarms due to their asymmetric structure.

After computing the CPS parameters along all best-tracks (once in JRA-55 and once in ERA-Interim), we applied the CPS criteria to detect "ET storms", i.e., storms that begin and complete the transition from a tropical to an extratropical system. The resulting classification into ET storms and non-ET storms lies at the core of this study.

c. Statistical Performance Measures

To measure how well the CPS-based climatology matches the observed ET storms, we use the only available observational data: the 'storm type' labels in the best-track archives, which represent the classification proposed by the specialists at the operational warning centers. Despite the known issues (see section 4) and subjective nature of these labels (they are mainly based upon analysis of satellite images), we treat them as the "true" classification of ET storms. Consequently, the performance of the CPS-based ET detection is assessed by comparing its predicted ET events to the ET events in the best-track labels, both by (visually) checking the agreement on individual storms as well as by applying statistical performance measures. Two commonly used statistical

performance metrics for classification algorithms are precision and recall (Ting 2010), which are defined as follows:

$$\text{precision} = \frac{\text{true positives}}{\text{true positives} + \text{false positives}}$$

$$\text{recall} = \frac{\text{true positives}}{\text{true positives} + \text{false negatives}}$$

Precision is the ratio of correctly predicted positive observations (here: ET storms) to the total predicted positive observations and answers the question, 'Of all storms the CPS-detection declares to have undergone ET, how many are true ETs?' Recall is the ratio of correctly predicted positive observations to all observations in the actual class – the corresponding question is 'Of all true ET storms, how many does the CPS-detection label as such?' The harmonic mean of precision and recall is called the F1 score and allows to quantify the overall performance of the CPS ET detection in a single number:

$$\text{F1} = 2\frac{\text{precision} \times \text{recall}}{\text{precision} + \text{recall}}$$

F1 score, precision and recall all range from 0 to 1, with higher scores signaling better performances.

3. Results

a. Building Blocks: CPS Parameters and Trajectories

Before zooming out to a global view on ET, let's examine the CPS parameters and the trajectories they trace out in the phase space. Box plots of all six-hourly CPS parameters (Fig. 2) show that both thermal wind parameters clearly have most of their probability distributions above the zero value, indicating the dominant presence of warm-cored storms. The distributions of the B parameter are concentrated around zero, representing the fingerprint of thermally symmetric tropical storms. As we will show in section 3.b, the long tails extending into the extratropical parameter

ranges in the NAT and the WNP (right tails for the B parameter, left tails for $-V_T^L$ and $-V_T^U$) will manifest themselves in high ET fractions in these two basins.

Due to the thresholds for asymmetry and cold-core structure, all CPS trajectories of transitioning storms exhibit some level of similarity. In general, though, individual trajectories of cyclones in the CPS are very diverse, demonstrating the wide range of possible structural evolutions the storms can follow. Apart from the high degree of inter-storm variability, the CPS path for a given storm may also differ quite substantially depending on which dataset was used to calculate the CPS parameters. Fig. 3 illustrates this dependence using the example of Tropical Storm Earl (1992), whose trajectory in a B vs.$-V_T^L$ cross section of the CPS (Figs. 3a and 3b) looks markedly different for the two reanalyses used in this study. Earl does not undergo ET in JRA-55, while the ERA-Interim trajectory depicts a full transition to an extratropical system (for reference, Earl also becomes extratropical in the NHC best-track data, albeit only at the last recorded time step).

On 06 UTC 3 Oct (the third-last track point), Earl is clearly visible in the relative vorticity fields at 850 hPa (Figs. 3c and 3d) of the two reanalyses, which feature a vortex centered northeast of Florida. The peak values are higher in ERA-Interim, but the differences in position and size of the storm in the two reanalyses are much too small to explain the discrepancy in the CPS trajectories.

As expected from the $B - V_T^L$ trajectory, the ΔZ profile (Fig. 3e) of JRA-55 decreases with height in the 900-600 hPa layer, indicating a warm core in the lower troposphere. This is consistent with the storm's position in the upper right 'asymmetric warm-core' quadrant of the CPS. In contrast, the ERA-Interim profile shows increasing geostrophic wind (and thus a cold-core structure) throughout the 900-300 hPa layer – consequently, the storm is located in the upper left 'extratropical' quadrant.

The following sections will make it clear that such differences between JRA-55 and ERA-Interim are not only visible in individually selected storms but also in the outcomes of climatological analyses.

b. Global Climatology of ET

1) FRACTION

Fig. 4 juxtaposes observed and CPS-computed global ET fractions. Note that the CPS-derived ET fractions in Fig. 4 refer to the time periods for which best-track labels were available – in the case of the JTWC best-tracks, the available period is 2003-2015. An overview of all CPS-derived fractions for the entire time period 1979-2015 can be found in Table 2.

There are several notable differences between ocean basins as well as between the two reanalysis datasets: According to the JMA and NHC best-track data, 48% of the storms in the WNP and 45% of the storms in the NAT undergo ET. Compared to these two basins, ET is very rare in the ENP and the NI (2.8% and 1.5%, respectively). The low ET fraction in the ENP is mostly the result of a strong subtropical ridge over southwestern North America, which exerts its influence over much of the hurricane season and tends to steer the cyclones westward away from land (Wood and Ritchie 2014). In the NI, northward moving storms usually make landfall before reaching a sufficiently baroclinic environment to undergo transition. Of the SH basins, the SP (44%) has a considerably higher ratio of ET storms than the SI (27%) and the AUS (20%).

The CPS-computed fractions derived based on JRA-55 match the observed fractions pretty closely in all basins. With the exceptions of the SP and the SI, the ERA-Interim fractions exceed the JRA-55 values and the observations, particularly in the ENP and the NI. This pattern is robust even when considering the sensitivity to various definitions of ET onset and ET completion, e.g., when varying the V_T^L and V_T^U thresholds from 0 to -10.

ET fractions depend not only on the basin and the reanalysis dataset, but also on the best-track archive: In the WNP, the percentage of storms undergoing ET in the JMA dataset exceeds that in the JTWC dataset by 6.4 percentage points (Fig. 4). This discrepancy is even more pronounced in the objective, CPS-based ET fractions, indicating that its primary reason lies in the tracks themselves rather than in different operational practices at the warning centers. Indeed, Fig. 5 reveals that the JMA best-tracks extend further northeast: Their average end position is 32°N, 141°E (standard deviation: 14°, 28°), while the average JTWC best-track ends at 28°N, 131°E (standard deviation: 10°, 22°). Thus, the JMA storms veer more frequently into the midlatitude zone where ET usually happens. Of all cyclones that undergo ET along the JMA best-track but not along the JTWC best-track, about 80% complete ET further north than the latitude of the last JTWC track point. Given that the JMA labels are available over a longer time period and that the JMA best-tracks have a better performance than the JTWC best-tracks (as shown in the second part of this study), all results for the WNP presented in the rest of this study are based on the JMA archive.

Past studies on ET climatologies have mostly focused on single ocean basins and differ significantly in their methods (e.g., some of them apply objective techniques such as the CPS while others use warning center labels or satellite images), as shown in the papers summarized in Table 3. The large difference between the estimates for the WNP obtained by Klein et al. (2000) and Kitabatake (2011) illustrates the dependence of the ET climatology on the methodology, dataset, time period, and sample size.

Our ET percentage of 46.7% for the WNP obtained from JRA-55 is comparable to the value of 40% in Kitabatake (2011), who used the JRA-25 reanalysis. Tracking North Atlantic storms in ERA-Interim, Zarzycki et al. (2016) computed an ET fraction of 55.2%, which agrees very well with the fraction of 53.7% yielded by our ET detection in the NAT best-track storms in ERA-Interim.

According to Wood and Ritchie (2014), 9% of the storms in the ENP undergo ET, which is about twice the 4.8% we obtain using the same dataset and a similar time period. This difference is mainly a consequence of the fact that Wood and Ritchie used a definition of ET which did not require V_T^U to cross any threshold. Indeed, if we remove the condition on V_T^U, the calculated ET fraction in the ENP rises to 8.0%. Thus, a lower-tropospheric cold core is not necessarily preceded by the development of a cold core in the upper troposphere – in other words, the requirement for an upper-tropospheric cold-core for ET completion is not a redundant criterion. In fact, with the notable exception of the NAT, the effect of ignoring the V_T^U parameter in the definition of ET completion is even larger in other ocean basins, especially for ERA-Interim. The original CPS framework presented in Hart (2003) had been tailored to the NAT, and in that basin, the ET rates are not sensitive to the upper-tropospheric parameter. However, considering that there is no absolute truth in the definitions of ET onset and completion, the requirement on the upper-tropospheric thermal structure in the definition of ET completion has been added in this study because it clearly improves the agreement with the best-tracks on a global basis.

Studholme et al. (2015) analyzed northern hemisphere storms tracked in ERA-Interim. Using a combination of CPS and a k-means clustering, they accounted for multiple pathways of ET. This approach resulted in ET fractions that are higher than the values of other climatologies (including the one presented here).

2) Seasonal Cycle

There is substantial variability in the seasonal patterns of ET events in the different basins (Fig. 6). However, as there is a good agreement between the two reanalyses, Fig. 6 only shows the results for JRA-55. In the NAT, the number of ET storms is highest in September, but the ET fraction only reaches its peak in November. A very similar seasonal cycle was obtained by Hart

and Evans (2001) based on the storm type labels in the NHC best-tracks. The observed increase in ET fraction from summer to fall is explained by the combined effect of the delayed warming of the ocean and seasonal changes in the region that is conducive to growth of baroclinic instabilities (e.g., Hart and Evans 2001): In summer, a TC leaving the area that supports tropical development often can't reach a baroclinically favorable region before weakening too much for a transition to occur. In later months, however, this gap closes because the baroclinically favorable region pushes southward and encroaches on the area over which tropical development can occur – due to the large heat capacity of the ocean, this "tropically favorable" region still extends relatively far north at that time of the year. Thus, the environment is most ET-friendly in October and November, which is consistent with the increased transition probability in these months.

The WNP shows a double peak in May and September, which is consistent with the result of Kitabatake (2011). In contrast to the other basins, the WNP has TCs forming all year round, but the months that overlap with the NAT hurricane season (June - November) show a similar drop of the ET percentage in summer, followed by higher values in fall. Though, while the transition probability in the WNP decreases after September, it continues to rise in the NAT until the end of the season. This decrease of the ET fraction in the WNP during September-November coincides with the presence of high vertical wind shear in large parts of the basin, which restricts the formation of TCs to the Pacific warm pool and low latitudes. However, storms that recurve (and are more likely to undergo ET) tend to form further north (Camargo et al. 2007) and are thus underrepresented in late fall. Since the WNP's even higher peak of the ET fraction in May is not associated with a particularly high occurrence of recurving storms, it follows that the ET probability of recurving storms in that month must be relatively large, which was also noted by Kitabatake (2011).

The SH basins exhibit much less pronounced seasonal cycles of ET than the NAT or the WNP. In the SH, the extension of the subtropical jet into tropical latitudes acts to constrain the tracks of

TCs to lower latitudes than in the northern hemisphere (Krishnamurti et al. 2013). In addition, the seasonal change of the baroclinic energy source is relatively small except near the Antarctic (Zhu 2003). Thus, throughout the year, TCs in the SH encounter a fairly strong baroclinic environment already at low latitudes.

The NI and the ENP basins have very low ET rates and do not show a clear seasonality.

3) Interannual Variability

Time series of ET fractions (Fig. 7) reveal the interannual variability in the percentages of storms undergoing ET. The magnitudes of the year-to-year fluctuations in each basin reflect the variances in the distributions of the annual ET counts, which are driven by variances in the fraction of TCs that transition and the annual TC counts. For example, the variability in the NI is dominated by the combination of a low ET fraction and a low overall storm count. Except for the JRA-55 time series in the SI, the slopes of the linear regression lines are not statistically significant at the 95% confidence level (see Table 4).

Analyses in each basin of the best-track time series of ET fractions using a Poisson model of constant annual-mean TC formation and a constant probability per TC of undergoing ET suggest that the interannual variability is largely consistent with a stationary random process in the NAT, WNP, AUS, and the SI (not shown). Also, there is no significant lag-one autocorrelation in any of these time series (not shown), indicating the absence of year-to-year memory in the transition probability. Due to low ET and/or total TC counts, autocorrelation and consistency with a Poisson process were not evaluated for the ENP, NI, and the SP.

The correlations between the time series of JRA-55 and ERA-Interim (Table 4) are high and statistically significant for the NAT and the WNP. In the three SH basins and the NI, the correlations between the ET fractions in the two reanalyses are also statistically significant, but weaker.

Further, the higher overall ET fractions associated with the ERA-Interim-based calculation of CPS parameters (Fig. 4 and Table 2) are present in nearly all individual years.

4) Spatial Patterns

Defining the track density as the sum of all best-track data points located in each $1.25^\circ \times 1.25^\circ$ grid box, Fig. 8 compares the spatial distributions of ET storms with those of non-ET storms, using the JRA-55 classification. Track densities for ERA-Interim (not shown) qualitatively agree well with those of JRA-55. Due to the scarcity of ET events in the NI and the ENP, this part of the analysis focuses on the NAT, the WNP, and the SH. In the NAT and the WNP, ET storms recurve to a greater extent than the non-ET storms, which typically follow an east-west path with less poleward drift. As a result of this recurvature, the highest density of ET storms in the WNP is found in the East China Sea, while the concentration of non-ET storms peaks further southwest, in the South China and Philippine Seas. Although the track density in the NAT is more evenly spread throughout the basin than in the WNP, the general pattern is similar: ET storms most frequently pass the area off the coast of the southeast United States, and non-ET storms have their highest density southwest of that area, in the Gulf of Mexico.

Most SH storms that undergo ET occur northeast of Australia, mainly in the SP. This is a region where the density of non-ET storms is rather low compared to the SI and the western part of the AUS. Thus, the storms passing that area have a high probability of transition. Indeed, as shown in Fig. 4, the ET fraction in the SP is about 40%, significantly higher than in the SI and the AUS, where on average only about every fifth storm undergoes ET.

The genesis locations of ET storms and non-ET storms (not shown) don't differ dramatically. In particular, there is no strongly localized "hot spot" of ET storm formation in any northern hemisphere basin – in fact, the genesis positions of ET storms in the NAT and the WNP are

overall more homogeneously distributed than those of their non-ET counterparts. However, this relatively even spread of genesis locations in the cumulative view does not preclude the existence of seasonal variations (e.g., such as those found in the NAT by Hart and Evans 2001). The SH ET storms predominantly form in the SP, which is the region where we also find the highest track density of ET storms.

Statistics of the latitudes where TCs complete their transitions into extratropical cyclones are given in Fig. 9. The median latitude of ET completion in the seven basins ranges from about 20° to 40°, and these inter-basin variations are substantially greater than the differences between the two reanalyses.

In the NAT and the WNP, ET completion takes place substantially further poleward than in the other basins. Furthermore, the decomposition into monthly statistics reveals the presence of a distinct annual cycle in the ET latitude in both basins: Transition occurs at higher latitudes during the peak of the season and shifts to lower latitudes during the early and later months. In the NAT, these seasonal patterns of ET latitude are negatively correlated with those of the ET fractions (Fig. 6), i.e., months with high ET rates (e.g., November) have lower latitudes of ET completion, and vice versa. The correlation is not as strong in the WNP, where the decreasing ET latitudes in October-December are not associated with an increase in ET fraction. This is consistent with the idea that the WNP is dominated by straight-moving storms at that time of the year.

The SH ETs occur at lower latitudes than in the NAT and the WNP and don't have a distinct seasonal pattern. These features are consistent with the narrower latitudinal extent of the TC tracks in the SH, which reduces the exposure to the seasonal effects of advancing and retreating regions of baroclinic activity.

5) LANDFALL

TC damage largely depends on landfalling storms, and some of these storms undergo ET before, while, or after they hit the coast. Table 5 provides a summary of the landfall events recorded in the best-track data, dividing the storms into tropical storms, transitioning storms, and extratropical storms (i.e., storms that have completed ET). Note that this classification refers to the nature of a storm at the time when the landfall occurs and does not make any statement on its further structural evolution – e.g., a TC that does not show any signs of a transition when reaching land might still undergo ET at a later stage despite falling into the 'tropical' category in Table 5. Also, we only count the most intense landfall of each storm.

As a result of the geometry of the basins and the predominant large-scale circulation, the landfall rates span a large range: At the extreme ends, almost three out of four storms in the NI move over land, but only about one out of seven in the ENP and the SP. In all basins, storms with tropical characteristics account for a clear majority of all landfall events, and in most cases the storm categories of JRA-55 and ERA-Interim agree relatively well. However, there is a discrepancy between JRA-55 and ERA-Interim in the ENP: According to the JRA-55-based CPS parameters, nearly all landfalling storms are symmetric and warm-cored, while ERA-Interim classifies a fifth of them as extratropical. This suggests that ERA-Interim's higher overall ET fraction (Fig. 4) is the result of TCs that undergo ET over the ocean, rather than a consequence of structural changes in the wake of landfalls that might push storms into the asymmetric region of the CPS or increase the average position difference between the storm center in the best-tracks and in the reanalysis.

The "classification mismatch" between JRA-55 and ERA-Interim has the same general pattern in all basins: JRA-55 declares more landfalling storms to be of tropical nature than ERA-Interim. In the ENP, about 25% all landfalling storms are considered transitioning or extratropical in the

ERA-Interim classification, but less than 4% according to JRA-55. It is also notable that in terms of absolute numbers, the difference in the WNP – 103 transitioning or extratropical storms in JRA-55, compared to 171 in ERA-Interim – is even higher than that in the ENP.

Considering storm counts and percentages, coastal regions in the NAT and the WNP are most frequently affected by transitioning or extratropical storms. During the 1979-2015 period, such landfall events happen 1-2 times per year in the NAT, and 3-5 times per year in the WNP.

In most basins, the classification of landfalling storms resulting from the best-track labels yields substantially smaller percentages of extratropical storms than either of the two reanalyses.

Fig. 10 shows all storms that are transitioning or extratropical at the time of their most intense landfall. The locations of ET completion in the WNP are clustered in a region between about 25°N and 45°N centered over Japan, whereas completion in the NAT happens preferentially along the east coast of the United States and Canada. In both basins, the tracks in Fig. 10 represent about 60% of the total landfalling storms that undergo ET at some point in their lives – i.e., approximately 40% of the storms in this group only begin to transition after landfall. When staying over land, such "post-landfall transitioners" can still cause substantial damage (e.g., Sousounis and Desflots 2010).

In the SH, landfalling ET storms mainly pose a threat to the AUS, especially to Western Australia and the islands in the Coral and Tasman Seas. However, with a frequency of about one ET landfall every 2-4 years, the risk is substantially smaller than in the NAT or the WNP.

6) Transition period and ET time

Defining the transition period as the time between the onset ($B > 11$) and the completion ($-V_T^U < 0$ and $-V_T^L < 0$) of ET, we find that in most basins, the average ET takes between 1 and 2 days (Table 6). However, comparing the transition periods between individual basins is not

possible due to the large inter-reanalysis differences – e.g., in the WNP, the CPS parameters from ERA-Interim yield a mean transition period of 56 h, which is one day longer than the average ET duration in JRA-55. With the exception of the NAT, the transition periods in ERA-Interim are longer than those of JRA-55 in all other basins as well.

Evans and Hart (2003) obtained a mean transition period of about 33 h for the NAT, which agrees well with the 35 h (38 h) from ERA-Interim (JRA-55). On the other hand, our results for the WNP clearly exceed the average ET duration of about 17 h found by Kitabatake (2011).

There is an important caveat to be aware of in this examination of transition periods: For TCs that undergo ET by first developing a cold-core structure before becoming asymmetric, the ET onset coincides with the ET completion, resulting in a transition period of 0 h. This issue was also noted by Kitabatake (2011). The statistics in Table 6 include all these cases – when they are removed, the mean transition period in each basin typically increases by about 10-20 h.

In order to analyze the timing of ET, probability density functions (PDFs) of the differences between the best-track ET times (as defined by the operational warning centers) and the times of ET completion in the CPS were calculated using a Gaussian kernel density estimation (Fig. 11). These PDFs are based on the set of all ET events that were identified both in the CPS and in the best-track archives. The distributions in the NAT are broader than in the WNP and the SH, indicating a higher variance in the declared ET time between the CPS and the NHC than between the CPS and the JMA or the JTWC. While the mean difference between the ET time in JRA-55 and that of the NHC labels is almost zero, ERA-Interim on average declares ET completion about 20 h before the NHC assigns the first 'extratropical' label. The JRA-55 ET completion times also agree slightly better with the JMA labels in the WNP, while the PDFs of the ET time differences to the JTWC labels in the SH are almost identical for the two reanalysis datasets.

c. Comparison: ET in CPS vs. ET in the Best-Tracks

A storm-by-storm evaluation of the ET detection in CPS against the best-track labels reveals that there are many correct classifications (true positives and true negatives, marked by green and blue dots) compared to the false positives and false negatives (red and magenta dots) in the NAT and the WNP (Fig. 12). Thus, the good agreement between the CPS-based ET fractions with the observations in those two basins is not a result of chance, but of the correct classification of individual storms. In fact, in the case of the JTWC best-tracks in the WNP (not shown), the storm-by-storm analysis reveals a pattern with many mismatches between the CPS and the best-track labels, despite the similar overall ET fractions.

A visual examination of the pattern of dots in Fig. 12 shows that the majority of false positives is located north of 20°N, but that they can occur as far south as 7°N (ERA-Interim, WNP). We also note the absence of any obvious systematic differences in the spatial distribution of the wrongly classified storms between the two reanalyses. Overall, a visual inspection would likely attribute a higher percentage of correct classifications to the JRA-55 based ET detection than to the ERA-Interim detection. This conclusion becomes much more evident in the case of the ENP. Here, the ET detection in JRA-55 clearly matches the observations much better, showing only a few scattered false positives whereas ERA-Interim features many red dots off the west coast of Mexico. Hence, ERA-Interim's overestimation of the ET fraction in the ENP is the result of wrongly classified ET events that occur over the ocean, as already mentioned in section 3.b.5. This proneness to false positives is also manifest in the box plots of the CPS parameters in the ENP (Fig. 2) – compared to their counterparts in JRA-55, the distributions of all three parameters in ERA-Interim have higher fractions of the overall probability in the extratropical range (i.e., $B > 11$, $V_T^L < 0$, $V_T^U < 0$).

For the SH, the distribution as well as the number of wrongly classified storms are very similar in the results for JRA-55 (Fig. 13) and ERA-Interim (not shown). There is a zonal band of true negatives with false positives at its southern edge, which implies that the CPS detection tends to declare ET more readily and further north than the JTWC. At the same time, though, the CPS detection also fails to identify ET events that happen significantly further south, as indicated by the false negatives poleward of 30°S.

ET in the NI (Fig. 13) is more difficult to assess due to the blocking effect of the continental land mass, which prevents storms from moving far enough north to undergo ET. From 2003 to 2015, the JTWC only labeled one single storm as extratropical. As a result, the evaluation of ET detection in the NI proved most sensitive to changes in the threshold values of the CPS parameters – e.g., the ET detection in JRA-55 perfectly matches the observations when applying a V_T^L value of -10 as a criterion for ET completion.

Fig. 14a shows the F1 scores of the ET detection using both JRA-55 and ERA-Interim data. Evidently, the CPS classification agrees best with the observations in the WNP and the NAT, with F1 scores of 0.91 and 0.80 for JRA-55, and 0.88 and 0.80 for ERA-Interim. The previously mentioned differences between the JMA and the JTWC best-tracks for the WNP translate into substantially lower F1 scores for the JTWC-based ET detection. Compared to the F1 scores in the NAT and the WNP (JMA), the scores in the ENP, the NI and the SH basins are markedly lower for both reanalyis datasets – but while the values for ERA-Interim fall off to almost zero (F1 = 0.10 in the ENP), the ET detection in JRA-55 achieves higher scores and clearly outperforms ERA-Interim in these basins (even though the relatively high F1 score of 0.67 in the NI might have to be taken with a grain of salt due to the small number of storms and the rareness of ET events).

The decomposition of the F1 scores into precision and recall (Fig. 14b) reveals that the F1 scores in the NAT, the WNP and the SH basins are composed of almost equal values of precision

and recall – in other words, the CPS ET classification is equally good at avoiding false positives as at avoiding false negatives. The F1 performance in the NI and the ENP is much more asymmetric, with a clearly higher recall than precision. This is likely a result of the scarcity of ET events in these two basins, which favors false alarms.

4. Discussion

The choice of the reanalysis accounts for notable differences in the outcome of our analysis. The fact that JRA-55 is better suited to the task is consistent with Murakami (2014), where JRA-55 comes out ahead in an evaluation of the representation of TCs in six reanalyses. In addition, Wood and Ritchie (2014) mention that ERA-Interim has a bias toward cold-core values in the 900-600 hPa layer compared with both JRA-55 and the final operational global analysis (FNL) data from the Global Forecast System in the ENP. This bias leads to a high rate of false positives in that basin and was confirmed in our study. However, deficiencies in the representation of TCs are by no means limited to ERA-Interim but are a well-known issue of reanalyses (including JRA-55; e.g., Murakami 2014; Schenkel and Hart 2012) and climate model output (e.g., Camargo and Wing 2016; Randall et al. 2007) in general.

The most prominent issue associated with TCs in reanalyses is the substantial underestimation of the storm intensities. However, the fact that the CPS parameters are based on relative comparisons (layer thickness left and right of the storm for B, and vertical profiles of ΔZ for thermal wind parameters) rather than absolute values of variables like wind speed suggests that they are for the greatest part unaffected by the unrealistically weak intensities. To the extent this is true, this independence of the CPS parameters on absolute storm intensity also offers the hope that the threshold parameters used to detect ET may not have to be adjusted to the increasing resolution and stronger intensities of cyclones in future reanalyses.

Of course, the performance evaluation of the CPS-based ET detection presented in this study also hinges on the quality of the best-track data, in particular on the labels indicating the tropical or extratropical nature of each cyclone. Even though the best-tracks are the most accurate and comprehensive archives of historical TC data available, it should be kept in mind that they are still prone to considerable uncertainty, especially the components that are derived from a forecaster's subjective judgment (e.g., Landsea and Franklin 2013). The exact procedure determining whether a cyclone is considered tropical or extratropical varies among the different TC warning centers. Usually, the decision is based on a combination of satellite imagery, model forecast fields and other operational tools (e.g., the NHC routinely considers CPS diagrams). Sometimes there is also a "human dimension" that gets factored in, taking into account that public perception of the threat associated with a cyclone changes when the system is declared extratropical (Masson 2014). Finally, there may be inhomogeneities in the data quality due to agencies putting less effort into the classification of transitioning storms or stopping the tracking earlier in basins where ET storms do not pose a threat to land.

Given these limitations, it is clear that assessing the CPS-based ET detection against the best-track labels cannot in all cases be interpreted as a comparison with the "true" classification. However, the time series of ET fractions (Fig. 7) did not reveal any statistically significant trends at the 95% significance level that were robust between the two reanalyses, and neither did time series of the magnitude of the difference between the CPS-based fractions and the best-track labels (not shown). Trends were also absent in time series of the annual mean latitude of storm track end points (not shown). Taken together, these results indicate that operational procedures in the tracking and characterization of cyclones have been fairly consistent in the time period 1979-2015, which provides some reassuring evidence that the best-track labels can to a reasonable approximation be assumed to represent the "ET truth".

5. Summary and Concluding Remarks

This paper presents a global climatology of tropical cyclones (TCs) that undergo extratropical transition (ET) in the time period 1979-2015. The climatology is based on objective ET detection in the cyclone phase space (CPS), calculated from JRA-55 and ERA-Interim reanalysis data.

Our findings can be summarized as follows:

- ET fractions vary substantially between the seven basins examined here: At the top end, about half of the storms in the North Atlantic (NAT) and the Western North Pacific (WNP) undergo ET, followed by a transition rate of about 40% in the South Pacific (SP). ET occurs less frequently in the South Indian Ocean (SI) and the Australian region (AUS), where approximately every fifth storm transitions, and only in rare cases in the Eastern and Central North Pacific (ENP) and the North Indian Ocean (NI). In the NI, continental landmass stands in the way of northward moving storms, while a strong subtropical ridge over southwest North America generates a westward steering flow that prevents ET from occurring in the ENP.

- There are differences in the seasonal cycles of ET in the NAT, the WNP, and the SH basins: The ET fraction maximizes later in the NAT than in the WNP, but both basins exhibit a local minimum in the earlier part of the peak season. We suggest that the interplay of tropical and baroclinic regulation, which is thought to be responsible for the November peak in the NAT, might be a weaker determinant of the transition probability for the fall season in the WNP due to the prevalence of straight moving-storms at that time of the year. In the SH basins, the ET fractions vary much less throughout the season, which is conceivably related to the narrower meridional confinement of the tracks.

- With the exception of the SI, time series of annual ET fractions from 1979 to 2015 don't show any statistically significant trends at the 95% confidence level. This finding strengthens

the usability and interpretability of the transition probabilities presented here as long-term climatological averages.

- The choice of the reanalysis dataset used to calculate the CPS parameters has a substantial impact on the resulting climatology. Most notably, ET fractions derived in ERA-Interim in most cases exceed those calculated in JRA-55 (and often also the ET observations archived in the best-tracks), especially in the ENP.

- The objective ET detection in CPS based on JRA-55 has a higher skill (fewer false positives and false negatives) in the classification of ET storms and non-ET storms than does the ERA-Interim based detection. The difference is small for the NAT and the WNP, where the classification skill is similarly high for both reanalyses, but JRA-55 clearly outperforms ERA-Interim in the other basins. Thus, the fact that the ET fractions derived from JRA-55 match the observations better than the ERA-Interim fractions is not a statistical coincidence, but reflects an actual difference in classification skill.

- The lower performance of ERA-Interim is mainly due to a higher false alarm rate, which is especially pronounced in the ENP.

Due to the global scope and consistent method, the results presented in this study are well suited to serve as a benchmark for other studies including research on ET under climate change scenarios, or for applications in global hazard models.

Acknowledgments. The authors would like to thank Dr. Robert Hart for providing Grid Analysis and Display System (GrADS) scripts that facilitated the development of the Python code used in this study.

583 **References**

584 Agustí-Panareda, A., S. L. Gray, G. C. Craig, and C. Thorncroft, 2005: The extratropical tran-
585 sition of tropical cyclone Lili (1996) and its crucial contribution to a moderate extratropical
586 development. *Mon. Wea. Rev.*, **133 (6)**, 1562–1573, doi:10.1175/MWR2935.1.

587 Anwender, D., P. A. Harr, and S. C. Jones, 2008: Predictability associated with the downstream im-
588 pacts of the extratropical transition of tropical cyclones: Case studies. *Mon. Wea. Rev.*, **136 (9)**,
589 3226–3247, doi:10.1175/2008MWR2249.1.

590 Atallah, E. H., and L. F. Bosart, 2003: The extratropical transition and precipitation distribution
591 of hurricane Floyd (1999). *Mon. Wea. Rev.*, **131 (6)**, 1063–1081, doi:10.1175/1520-0493(2003)
592 131⟨1063:TETAPD⟩2.0.CO;2.

593 Camargo, S. J., A. W. Robertson, S. J. Gaffney, P. Smyth, and M. Ghil, 2007: Cluster anal-
594 ysis of typhoon tracks. Part I: General properties. *J. Climate*, **20 (14)**, 3635–3653, doi:
595 0.1175/JCLI4188.1.

596 Camargo, S. J., and A. A. Wing, 2016: Tropical cyclones in climate models. *Wiley Interdisci-*
597 *plinary Reviews: Climate Change*, **7 (2)**, 211–237, doi:10.1002/wcc.373.

598 Dee, D. P., and Coauthors, 2011: The ERA-Interim reanalysis: Configuration and performance of
599 the data assimilation system. *Quart. J. Roy. Meteor. Soc.*, **137 (656)**, 553–597, doi:10.1002/qj.
600 828.

601 Ebita, A., and Coauthors, 2011: The Japanese 55-year Reanalysis "JRA-55": An interim report.
602 *SOLA*, **7**, 149–152, doi:10.2151/sola.2011-038.

603 Emanuel, K., 2005: *Divine wind: The history and science of hurricanes*. Oxford University Press.

Evans, J. L., and R. E. Hart, 2003: Objective indicators of the life cycle evolution of extratropical transition for Atlantic tropical cyclones. *Mon. Wea. Rev.*, **131 (5)**, 909–925, doi:10.1175/1520-0493(2003)131⟨0909:OIOTLC⟩2.0CO;2.

Griffin, K. S., and L. F. Bosart, 2014: The extratropical transition of tropical cyclone Edisoana (1990). *Mon. Wea. Rev.*, **142 (8)**, 2772–2793, doi:10.1175/MWR-D-13-00282.1.

Hart, R. E., 2003: A cyclone phase space derived from thermal wind and thermal asymmetry. *Mon. Wea. Rev.*, **131 (4)**, 585–616, doi:10.1175/1520-0493(2003)131⟨0585:ACPSDF⟩2.0.CO;2.

Hart, R. E., and J. L. Evans, 2001: A climatology of the extratropical transition of Atlantic tropical cyclones. *J. Climate*, **14 (4)**, 546–564, doi:10.1175/1520-0442(2001)014⟨0546:ACOTET⟩2.0.CO;2.

Jones, S. C., and Coauthors, 2003: The extratropical transition of tropical cyclones: Forecast challenges, current understanding, and future directions. *Wea. Forecasting*, **18 (6)**, 1052–1092, doi:10.1175/1520-0434(2003)018⟨1052:TETOTC⟩2.0.CO;2.

Keller, J. H., 2012: *Diagnosing the downstream impact of extratropical transition using multi-model operational ensemble prediction systems*, Vol. 57. KIT Scientific Publishing.

Keller, J. H., 2017: Amplification of the downstream wave train during extratropical transition: Sensitivity studies. *Mon. Wea. Rev.*, **145 (4)**, 1529–1548, doi:10.1175/MWR-D-16-0193.1.

Kitabatake, N., 2011: Climatology of extratropical transition of tropical cyclones in the western North Pacific defined by using cyclone phase space. *J. Meteor. Soc. Japan. Ser. II*, **89 (4)**, 309–325, doi:10.2151/jmsj.2011-402.

Klein, P. M., P. A. Harr, and R. L. Elsberry, 2000: Extratropical transition of western North Pacific tropical cyclones: An overview and conceptual model of the transformation stage. *Wea. Forecasting*, **15 (4)**, 373–395, doi:10.1175/1520-0434(2000)015⟨0373:ETOWNP⟩2.0.CO;2.

Kobayashi, S., and Coauthors, 2015: The JRA-55 reanalysis: General specifications and basic characteristics. *J. Meteor. Soc. Japan. Ser. II*, **93 (1)**, 5–48, doi:10.2151/jmsj.2015-001.

Krishnamurti, T., L. Stefanova, and V. Misra, 2013: *Tropical Meteorology*. Springer Atmospheric Sciences, Springer New York, New York, NY, dOI: 10.1007/978-1-4614-7409-8.

Landsea, C. W., and J. L. Franklin, 2013: Atlantic hurricane database uncertainty and presentation of a new database format. *Mon. Wea. Rev.*, **141 (10)**, 3576–3592, doi:10.1175/MWR-D-12-00254.1.

Liu, M., G. A. Vecchi, J. A. Smith, and H. Murakami, 2017: The present-day simulation and twenty-first-century projection of the climatology of extratropical transition in the North Atlantic. *J. Climate*, **30 (8)**, 2739–2756, doi:10.1175/JCLI-D-16-0352.1.

Masson, A., 2014: The extratropical transition of hurricane Igor and the impacts on Newfoundland. *Natural hazards*, **72 (2)**, 617–632, doi:10.1007/s11069-013-1027-x.

Matano, H., and M. Sekioka, 1971: Some aspects of extratropical transformation of a tropical cyclone. *J. Meteor. Soc. Japan. Ser. II*, **49**, 736–743.

McTaggart-Cowan, R., J. R. Gyakum, and M. K. Yau, 2003: The influence of the downstream state on extratropical transition: Hurricane Earl (1998) case study. *Mon. Wea. Rev.*, **131 (8)**, 1910 – 1929, doi:10.1175//2589.1.

Murakami, H., 2014: Tropical cyclones in reanalysis data sets. *Geophys. Res. Lett.*, **41 (6)**, 2133–2141, doi:10.1002/2014GL059519.

Randall, D. A., and Coauthors, 2007: Climate models and their evaluation. *Climate change 2007: The physical science basis. Contribution of Working Group I to the Fourth Assessment Report of the IPCC (FAR)*, Cambridge University Press, 589–662.

Schenkel, B. A., and R. E. Hart, 2012: An examination of tropical cyclone position, intensity, and intensity life cycle within atmospheric reanalysis datasets. *J. Climate*, **25 (10)**, 3453–3475, doi:10.1175/2011JCLI4208.1.

Sinclair, M. R., 2002: Extratropical transition of Southwest Pacific tropical cyclones. Part I: Climatology and mean structure changes. *Mon. Wea. Rev.*, **130 (3)**, 590–609, doi:10.1175/1520-0493(2002)130⟨0590:ETOSPT⟩2.0.CO;2.

Sousounis, P., and M. Desflots, 2010: Evaluating the impacts of extratropical transitioning on typhoon losses via synoptic case studies. *Twenty-ninth Conference on Hurricanes and Tropical Meteorology*, Tucson, Arizona.

Studholme, J., K. Hodges, and C. Brierley, 2015: Objective determination of the extratropical transition of tropical cyclones in the Northern Hemisphere. *Tellus A*, **67 (0)**, doi:10.3402/tellusa.v67.24474.

Thorncroft, C., and S. C. Jones, 2000: The extratropical transitions of hurricanes Felix and Iris in 1995. *Mon. Wea. Rev.*, **128 (4)**, 947–972, doi:10.1175/1520-0493(2000)128⟨0947:TETOHF⟩2.0.CO;2.

Ting, K. M., 2010: *Precision and Recall*, 781–781. Springer US, Boston, MA, doi:10.1007/978-0-387-30164-8_652.

Wood, K. M., and E. A. Ritchie, 2014: A 40-year climatology of extratropical transition in the eastern North Pacific. *J. Climate*, **27 (15)**, 5999–6015, doi:10.1175/JCLI-D-13-00645.1.

668 Zarzycki, C. M., D. R. Thatcher, and C. Jablonowski, 2016: Objective tropical cyclone extra-
669 tropical transition detection in high-resolution reanalysis and climate model data. *Journal of*
670 *Advances in Modeling Earth Systems*, n/a–n/a, doi:10.1002/2016MS000775.

671 Zhu, Y., 2003: *Large-scale Inhomogeneous Thermodynamics – And Application for Atmospheric*
672 *Energetics*. Cambridge International Science Pub.

LIST OF TABLES

Table 1. Overview of the TC track data used in this study. The time period is 1979-2015 for all basins. 32

Table 2. Summary of ET fractions for the time period 1979-2015, derived in JRA-55 and ERA-Interim. Values are given as percentages and as number of ET storms out of the total number of storms in each basin. 33

Table 3. Literature overview of past studies on ET fractions in various basins (no claim to completeness) 34

Table 4. Statistics of the time series of ET fractions: Mean and standard deviation (JRA-55 / ERA-Interim), p-value of the slope of the linear regression lines (JRA-55 / ERA-Interim), Pearson correlation coefficient between the JRA-55 and the ERA-Interim time series, and p-value of that correlation coefficient. 35

Table 5. Overview of landfalling storms (1979-2015) and their characteristics at the time of the landfall. Based on the CPS parameters calculated in JRA-55 and in ERA-Interim, the landfalling storms in each basin are categorized into tropical (trop), transitioning (trans), and extratropical (extratrop) storms. For comparison, the categorization (tropical or extratropical) resulting from the best-track labels is shown as well. In parentheses, the number of landfalling storms is given as a percentage of total storms in each basin, and the storm counts in each category are given as a percentage of the total landfalling storms. Numbers that only refer to the time period 2003-2015 are marked with an asterisk. 36

Table 6. Statistics of transition periods: number of ET events (1979-2015), mean and standard deviation of the transition periods in each basin, for the JRA-55 and the ERA-Interim ET classifications. 37

TABLE 1. Overview of the TC track data used in this study. The time period is 1979-2015 for all basins.

Ocean basin	**Code**	**Source of best-tracks**	**# Storms**
North Atlantic	NAT	NHC	456
Western North Pacific	WNP	JMA, JTWC	941, 950
Eastern and Central North Pacific	ENP	NHC	610
North Indian Ocean	NI	JTWC	179
South Indian Ocean	SI	JTWC	334
Australian region	AUS	JTWC	377
South Pacific	SP	JTWC	225

TABLE 2. Summary of ET fractions for the time period 1979-2015, derived in JRA-55 and ERA-Interim. Values are given as percentages and as number of ET storms out of the total number of storms in each basin.

	JRA-55		**ERA-Interim**	
NAT	47.8%	(218/456)	53.7%	(245/456)
WNP (JMA)	46.7%	(439/941)	53.6%	(504/941)
WNP (JTWC)	28.3%	(269/950)	37.5%	(356/950)
ENP	4.8%	(29/610)	23.4%	(143/610)
NI	5.6%	(10/179)	13.4%	(24/179)
SI	11.1%	(37/334)	17.4%	(58/334)
AUS	13.5%	(51/377)	25.2%	(95/377)
SP	28.4%	(64/225)	36.0%	(81/225)

TABLE 3. Literature overview of past studies on ET fractions in various basins (no claim to completeness)

Basin	**Author(s)**	**ET fraction**	**Method / Data**	**Time period (# storms)**
NAT	Hart and Evans (2001)	46%	NHC best-track labels	1950-1996 (463)
NAT	Studholme et al. (2015)	68%	CPS and k-means clustering, storms tracked in ECMWF operational analysis	2000-2008 (72)
NAT	Zarzycki et al. (2016)	55%	CPS, storms tracked in ERA-Interim	1980-2002 (87)
WNP	Klein et al. (2000)	27%	Satellite imagery, NOGAPS	1994-1998 (112)
WNP	Kitabatake (2011)	49% 40%	JMA best-track labels CPS, JRA-25	1974-2004 (687)
WNP	Studholme et al. (2015)	65%	CPS and k-means clustering, storms tracked in ECMWF operational analysis	2000-2008 (111)
ENP	Wood and Ritchie (2014)	9%	CPS, JRA-55	1971-2012 (631)
ENP	Studholme et al. (2015)	35%	CPS and k-means clustering, storms tracked in ECMWF operational analysis	2000-2008 (81)
NI	Studholme et al. (2015)	31%	CPS and k-means clustering, storms tracked in ECMWF operational analysis	2000-2008 (32)
SI	Griffin and Bosart (2014)	44%	Subjective identification of ET cases in best-track data of Météo-France La Réunion, ERA-Interim	1989-2013 (235)
SP	Sinclair (2002)	32%	Based on # TCs reaching midlatitudes	1970-1996 (251)

699 TABLE 4. Statistics of the time series of ET fractions: Mean and standard deviation (JRA-55 / ERA-Interim),
700 p-value of the slope of the linear regression lines (JRA-55 / ERA-Interim), Pearson correlation coefficient be-
701 tween the JRA-55 and the ERA-Interim time series, and p-value of that correlation coefficient.

Basin	**mean [%]**	**stdev [%]**	**p-value of slope**	**corr. coeff. (Pearson)**	**p-value of corr. coeff.**
NAT	47.4 / 54.7	17.8 / 16.8	0.96 / 0.30	0.85	3.49E-11
WNP	46.9 / 53.6	9.8 / 9.7	0.17 / 0.31	0.90	5.06E-14
ENP	4.8 / 24.1	4.7 / 8.3	0.07 / 0.18	-0.11	0.52
NI	6.3 / 15.9	13.0 / 18.2	0.98 / 0.14	0.37	0.02
SI	11.3 / 17.7	12.3 / 14.3	4.91E-03 / 0.18	0.64	1.74E-05
AUS	13.6 / 25.4	10.4 / 12.7	0.27 / 0.77	0.50	1.48E-03
SP	27.5 / 34.5	23.9 / 21.9	0.07 / 0.59	0.53	7.79E-04

TABLE 5. Overview of landfalling storms (1979-2015) and their characteristics at the time of the landfall. Based on the CPS parameters calculated in JRA-55 and in ERA-Interim, the landfalling storms in each basin are categorized into tropical (trop), transitioning (trans), and extratropical (extratrop) storms. For comparison, the categorization (tropical or extratropical) resulting from the best-track labels is shown as well. In parentheses, the number of landfalling storms is given as a percentage of total storms in each basin, and the storm counts in each category are given as a percentage of the total landfalling storms. Numbers that only refer to the time period 2003-2015 are marked with an asterisk.

		JRA-55			**ERA-Interim**			**Best-Track Labels**	
Basin	Landfalling storms (% of total)	trop	trans	extra-trop	trop	trans	extra-trop	trop	extra-trop
NAT	205 (45.0%)	150 (73.2%)	20 (9.8%)	35 (17.1%)	142 (69.3%)	16 (7.8%)	47 (22.9%)	178 (86.8%)	27 (13.2%)
WNP	542 (57.6%)	439 (81.0%)	66 (12.2%)	37 (6.8%)	371 (68.5%)	99 (18.3%)	72 (13.3%)	530 (97.8%)	12 (2.2%)
ENP	85 (13.9%)	82 (96.5%)	1 (1.2%)	2 (2.4%)	64 (75.3%)	4 (4.7%)	17 (20.0%)	85 (100.0%)	0 (0.0%)
NI	134 (74.9%)	128 (95.5%)	3 (2.2%)	3 (2.2%)	119 (88.8%)	5 (3.7%)	10 (7.5%)	49* (100.0%)	0* (0.0%)
SI	77 (23.1%)	77 (100.0%)	0 (0.0%)	0 (0.0%)	76 (98.7%)	1 (1.3%)	0 (0.0%)	29* (100.0%)	0* (0.0%)
AUS	140 (37.1%)	131 (93.6%)	4 (2.9%)	5 (3.6%)	122 (87.1%)	5 (3.6%)	13 (9.3%)	44* (95.7%)	2* (4.4%)
SP	31 (13.8%)	23 (74.2%)	4 (12.9%)	4 (12.9%)	21 (67.7%)	6 (19.4%)	4 (12.9%)	5* (100.0%)	0* (0.0%)

TABLE 6. Statistics of transition periods: number of ET events (1979-2015), mean and standard deviation of the transition periods in each basin, for the JRA-55 and the ERA-Interim ET classifications.

	JRA-55			**ERA-Interim**		
	n_ET	mean [h]	stdev [h]	n_ET	mean [h]	stdev [h]
NAT	218	38	62	245	35	60
WNP	439	32	46	504	56	71
ENP	29	9	15	143	55	62
NI	10	24	35	24	33	46
SI	37	28	40	58	32	42
AUS	51	25	36	95	55	86
SP	64	27	40	81	34	58

LIST OF FIGURES

Fig. 1. Global best-tracks of TCs from 1990 to 2000, and the boundaries of the domains examined in this study. 40

Fig. 2. Box and whisker plots for the CPS parameters, calculated in JRA-55 and ERA-Interim. The box extends from the lower to the upper quartile, with a red line at the median, and the whiskers extend from the 5th to the 95th percentile. 41

Fig. 3. Trajectory of tropical storm Earl (1992) in a B vs. $-V_T^L$ cross section of the CPS. The CPS parameters in a) were calculated in JRA-55, while b) is based on ERA-Interim data. A and Z mark the beginning and end of the track, respectively. The magnitude of relative vorticity at 850 hPa in (c) JRA-55 and (d) ERA-Interim is shown on 06 UTC 3 Oct 1992, in units of 10^5 s^{-1}. The vertical profile of $\Delta Z = Z_{max} - Z_{min}$ within a 500 km radius about the reanalysis-specific storm center (e) is from the same date and time. 42

Fig. 4. Global ET fractions computed from the objective detection of ET in CPS (in JRA-55 and ERA-Interim) as well as from the storm type labels assigned in the best-track datasets. In the NAT, the WNP (JMA) and the ENP, the fractions are based on the period 1979-2015, while the fractions for the WNP (JTWC), NI, SI, AUS, and the SP refer to the period 2003-2015. The results for the WNP are shown for the best-track archives of JMA as well as JTWC. . . . 43

Fig. 5. TC tracks in the WNP (2000-2015), from the JMA (left) and the JTWC (right) best-track archives. 44

Fig. 6. Seasonal cycles of ET in terms of the average annual number of storms in each month (blue: total storms; orange: ET storms, calculated in JRA-55) for the time period 1979-2015. The black line refers to the percentage axis and shows the corresponding ET fraction, which is only calculated if a minimum of 10 storms (including non-ET storms) occurred in a given month over the whole time period. 45

Fig. 7. Time series of annual ET fractions from 1979 to 2015, for JRA-55 and ERA-Interim, with dashed lines representing the linear regression best fits to the time series. The vertical bars show the ET fractions derived from the best-track labels. 46

Fig. 8. Track density of ET storms and non-ET storms (as defined by the JRA-55 classification) in the NAT, the WNP, and the SH, showing the sum of all best-track data points falling into each $1.25^\circ \times 1.25^\circ$ grid box over the time period 1979-2015. 47

Fig. 9. Box plots of the absolute values of the latitudes at which storms complete ET, for all basins and all ETs in 1979-2015 (top; for JRA-55 and ERA-Interim), and decomposition into seasonal cycles for the NAT, WNP, SI, AUS, and the SP (for JRA-55). The box extends from the lower to the upper quartile, with a red line at the median, and the whiskers extend from the 5th to the 95th percentile. 49

Fig. 10. Tracks of storms that make landfall as transitioning or extratropical systems (according to the JRA-55 classification), for the time period 1979-2015. The yellow dots mark the locations of ET completion. 50

Fig. 11. Probability density functions of the differences between the best-track ET times and the ET completion in CPS, based on the ET events from 1979 to 2015 in the NAT and the WNP, and from 2003 to 2015 in the SH. The vertical lines indicate the means of the distributions, and the shaded regions represent values within one standard deviation about the mean. Positive

(negative) time differences indicate that the best-track ET time is later than (earlier than) the ET completion in CPS. 51

Fig. 12. Comparison of CPS-based ET detection with the best-track labels in the NAT, the WNP, and the ENP, using the JRA-55 (left column) and ERA-Interim (right column) classifications, for the time period 1979-2015. Each dot represents one storm: Green dots mark the position of ET completion for true positive storms (i.e., storms that were classified as ET storms in the CPS-based detection as well as in the best-track labels), red dots denote locations where false positive storms (i.e., storms that were classified as ET storms by the CPS but not by the best-track labels) completed ET, and the ET positions of false negative storms (i.e., storms that were classified as ET storms by the best-track labels but not by the CPS) are shown in magenta – here, the ET position is defined as the location where the storm is for the first time considered extratropical in the best-track data. Finally, the blue dots mark the locations where the true negative storms (which did not undergo ET in either of the two classification methods) acquire their lifetime maximum intensity. 52

Fig. 13. Comparison of CPS-based ET detection (using the JRA-55 classification) with the best-track labels in (a) the SH and (b) the NI, for the time period 2003-2015. The meaning of the dots and colors is the same as in Fig. 12. 53

Fig. 14. a) F1 scores assessing the performance of the CPS-based ET classification. In the NAT, the WNP (JMA) and the ENP, the F1 scores are based on the period 1979-2015, while the scores for the WNP (JTWC), NI, SI, AUS, and the SP have been calculated based on the period 2003-2015. The results for the WNP are shown for the best-track archives of JMA as well as JTWC. b) Precision and recall associated with the F1 scores in a); scores are marked as circles for JRA-55, and as triangles for ERA-Interim. 54

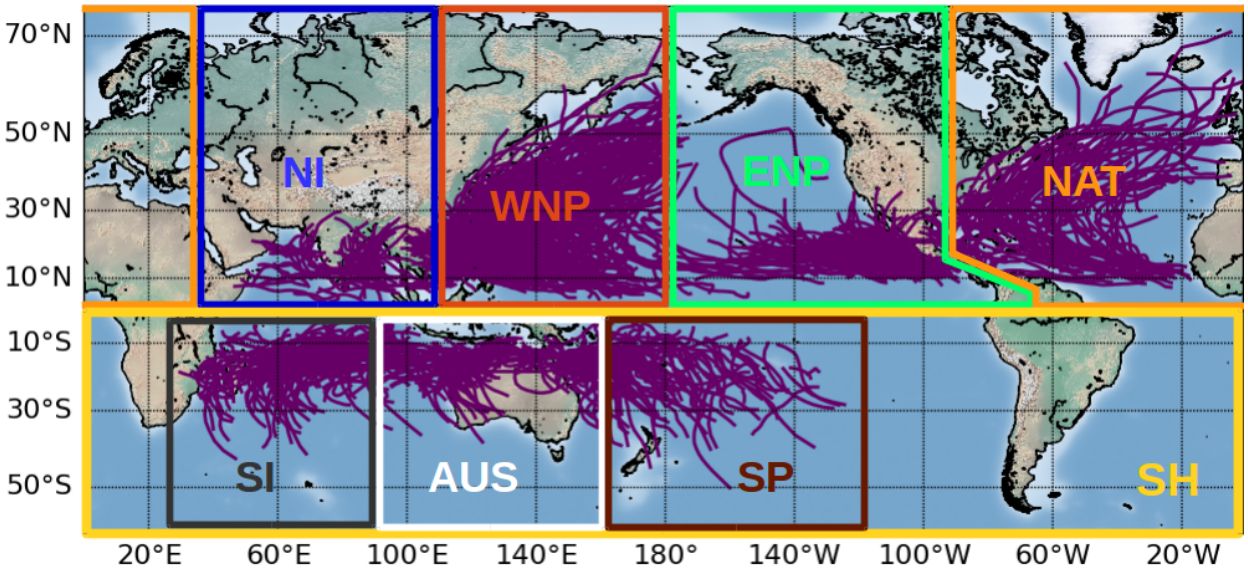

FIG. 1. Global best-tracks of TCs from 1990 to 2000, and the boundaries of the domains examined in this study.

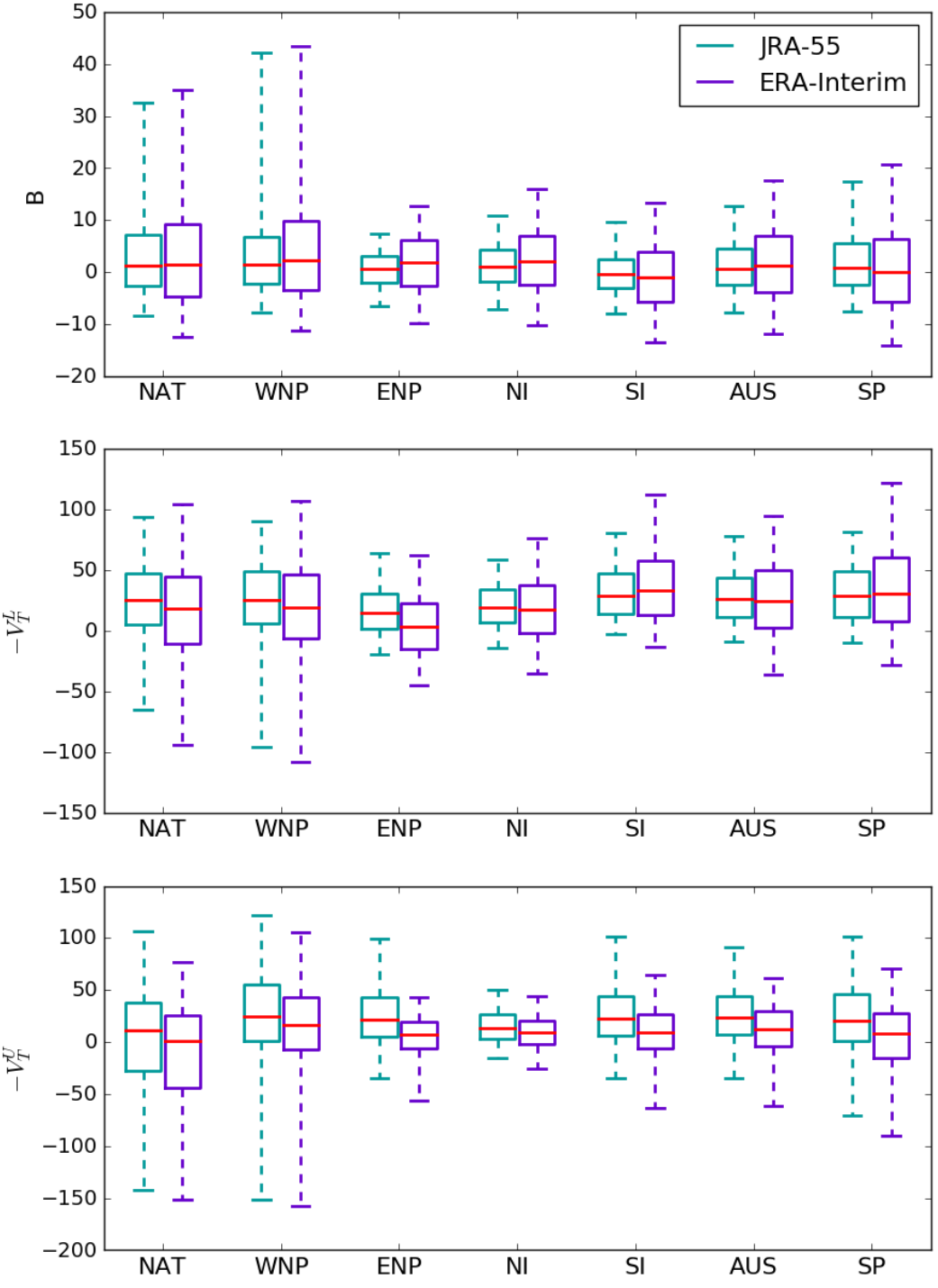

FIG. 2. Box and whisker plots for the CPS parameters, calculated in JRA-55 and ERA-Interim. The box extends from the lower to the upper quartile, with a red line at the median, and the whiskers extend from the 5th to the 95th percentile.

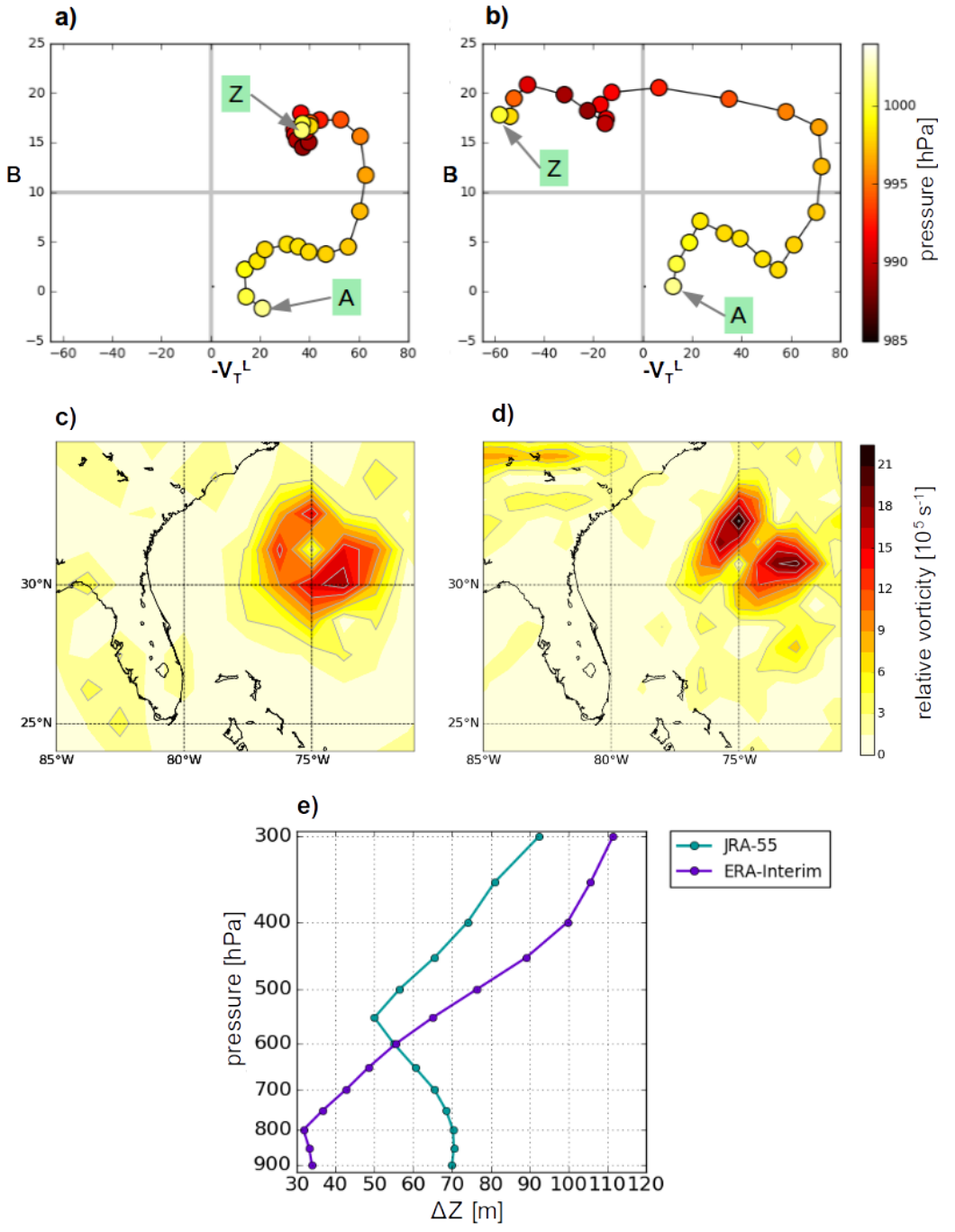

779 FIG. 3. Trajectory of tropical storm Earl (1992) in a B vs. $-V_T^L$ cross section of the CPS. The CPS parameters
780 in a) were calculated in JRA-55, while b) is based on ERA-Interim data. A and Z mark the beginning and end
781 of the track, respectively. The magnitude of relative vorticity at 850 hPa in (c) JRA-55 and (d) ERA-Interim is
782 shown on 06 UTC 3 Oct 1992, in units of 10^5 s^{-1}. The vertical profile of $\Delta Z = Z_{max} - Z_{min}$ within a 500 km
783 radius about the reanalysis-specific storm center (e) is from the same date and time.

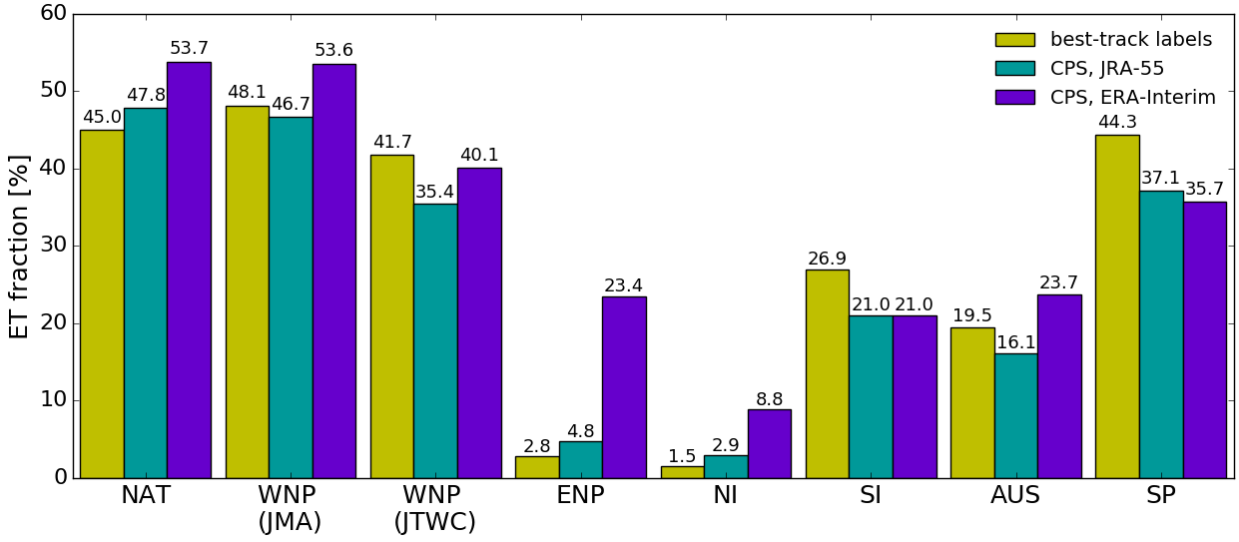

784 FIG. 4. Global ET fractions computed from the objective detection of ET in CPS (in JRA-55 and ERA-
785 Interim) as well as from the storm type labels assigned in the best-track datasets. In the NAT, the WNP (JMA)
786 and the ENP, the fractions are based on the period 1979-2015, while the fractions for the WNP (JTWC), NI, SI,
787 AUS, and the SP refer to the period 2003-2015. The results for the WNP are shown for the best-track archives
788 of JMA as well as JTWC.

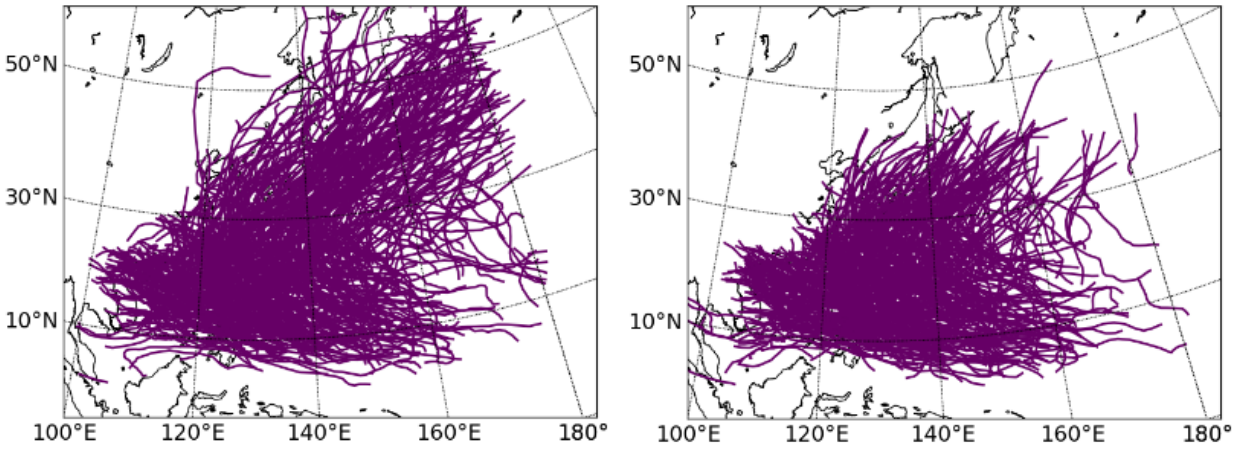

FIG. 5. TC tracks in the WNP (2000-2015), from the JMA (left) and the JTWC (right) best-track archives.

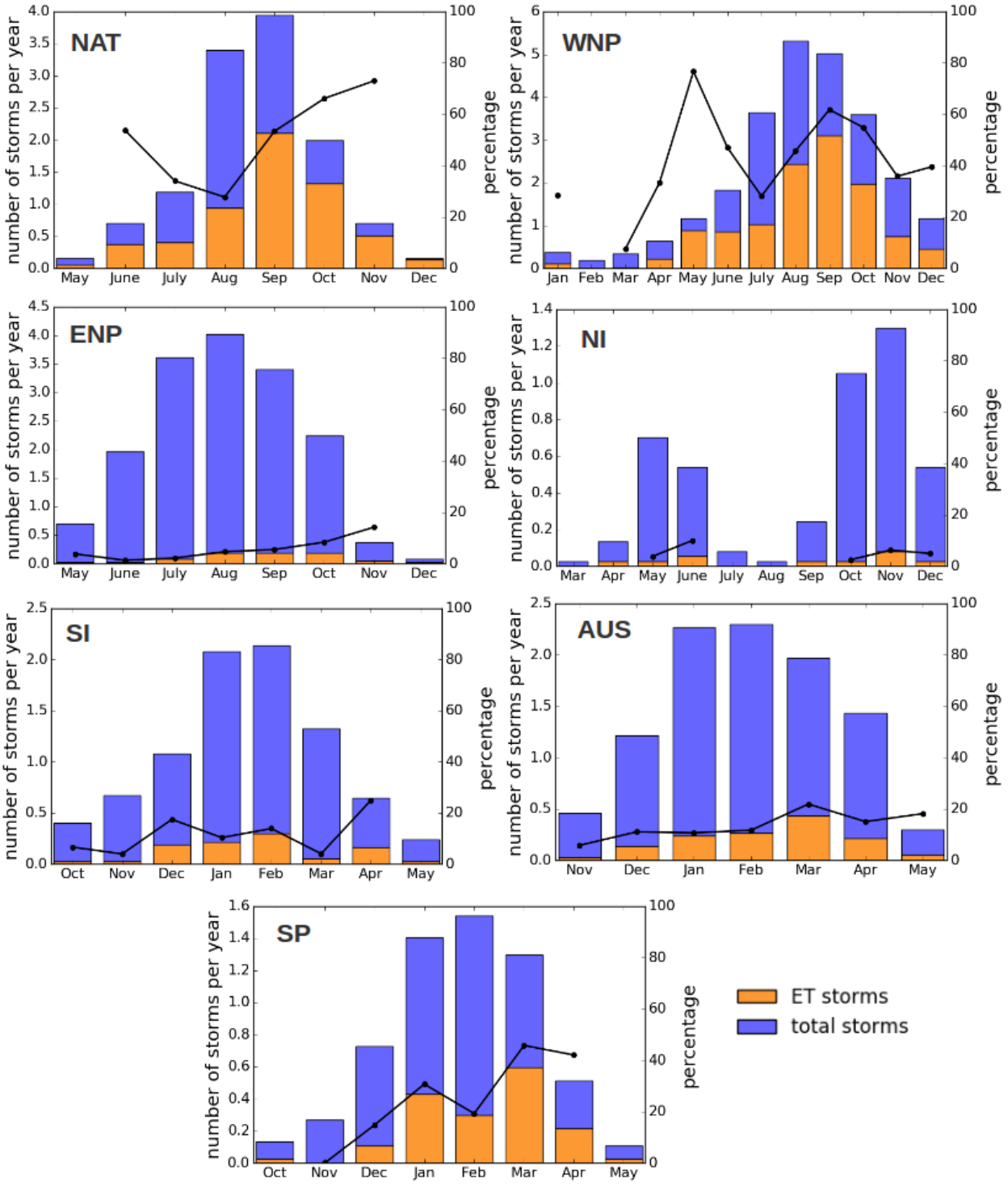

789 FIG. 6. Seasonal cycles of ET in terms of the average annual number of storms in each month (blue: total
790 storms; orange: ET storms, calculated in JRA-55) for the time period 1979-2015. The black line refers to the
791 percentage axis and shows the corresponding ET fraction, which is only calculated if a minimum of 10 storms
792 (including non-ET storms) occurred in a given month over the whole time period.

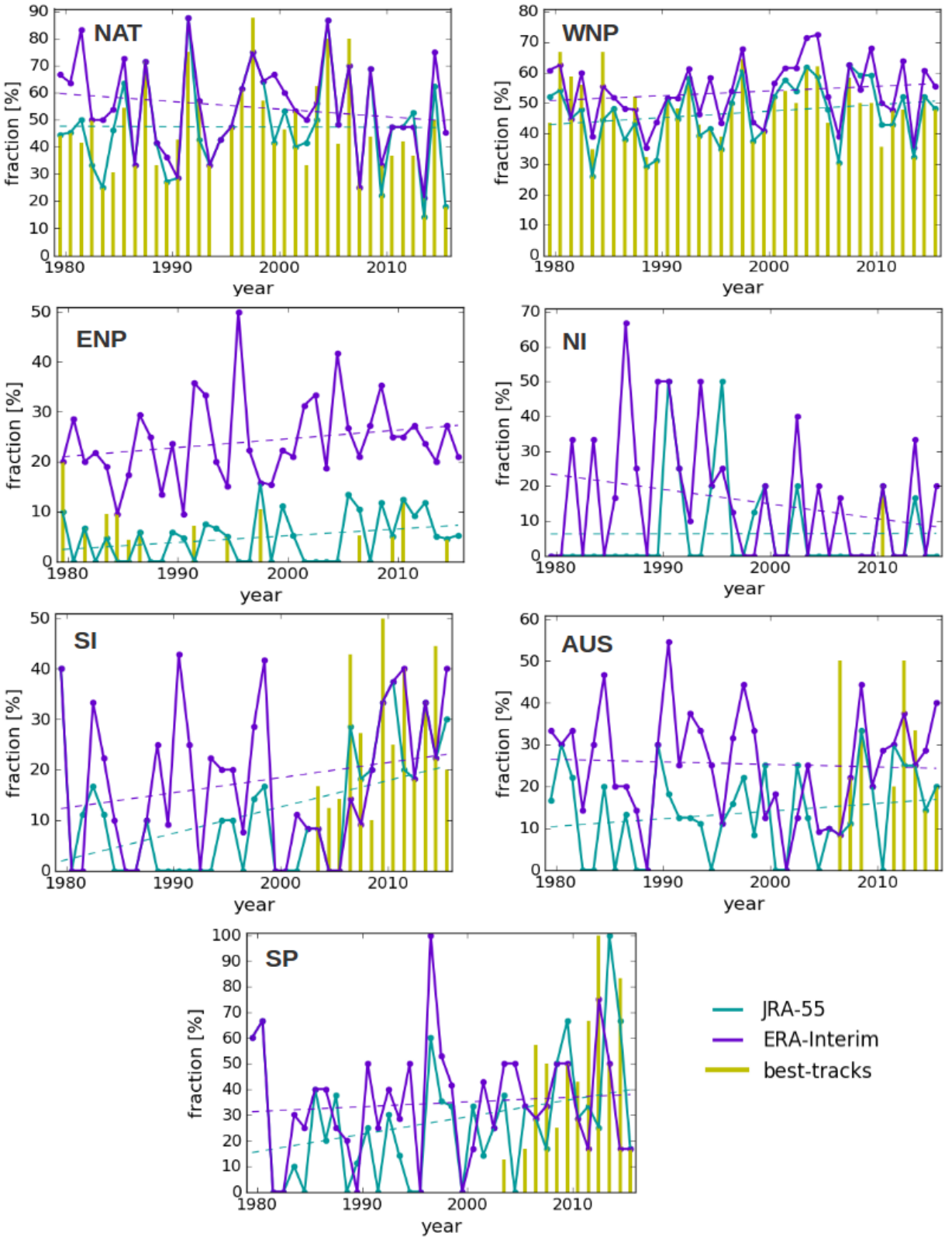

793 FIG. 7. Time series of annual ET fractions from 1979 to 2015, for JRA-55 and ERA-Interim, with dashed
794 lines representing the linear regression best fits to the time series. The vertical bars show the ET fractions derived
795 from the best-track labels.

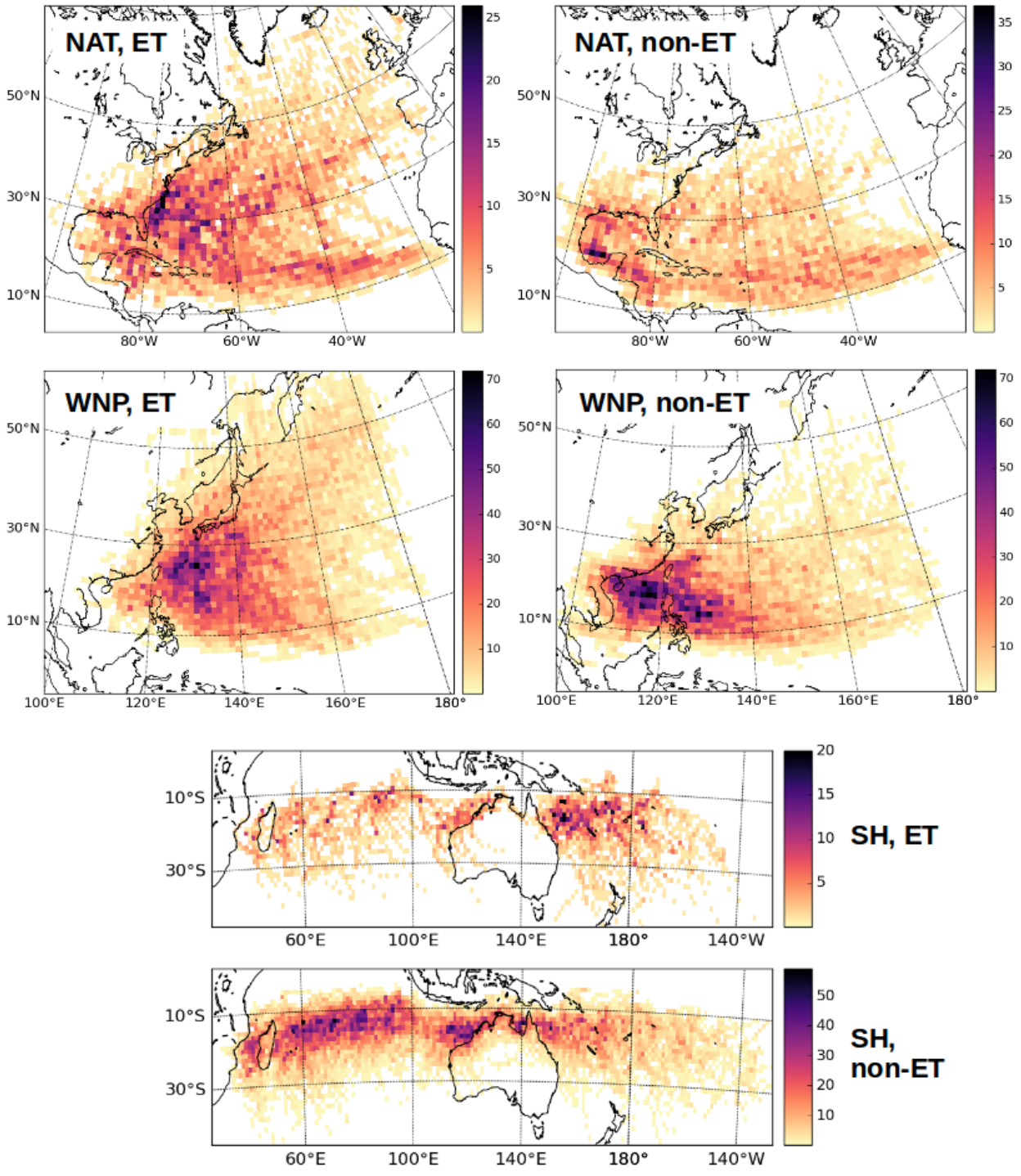

796 FIG. 8. Track density of ET storms and non-ET storms (as defined by the JRA-55 classification) in the NAT,
797 the WNP, and the SH, showing the sum of all best-track data points falling into each $1.25^\circ \times 1.25^\circ$ grid box over
798 the time period 1979-2015.

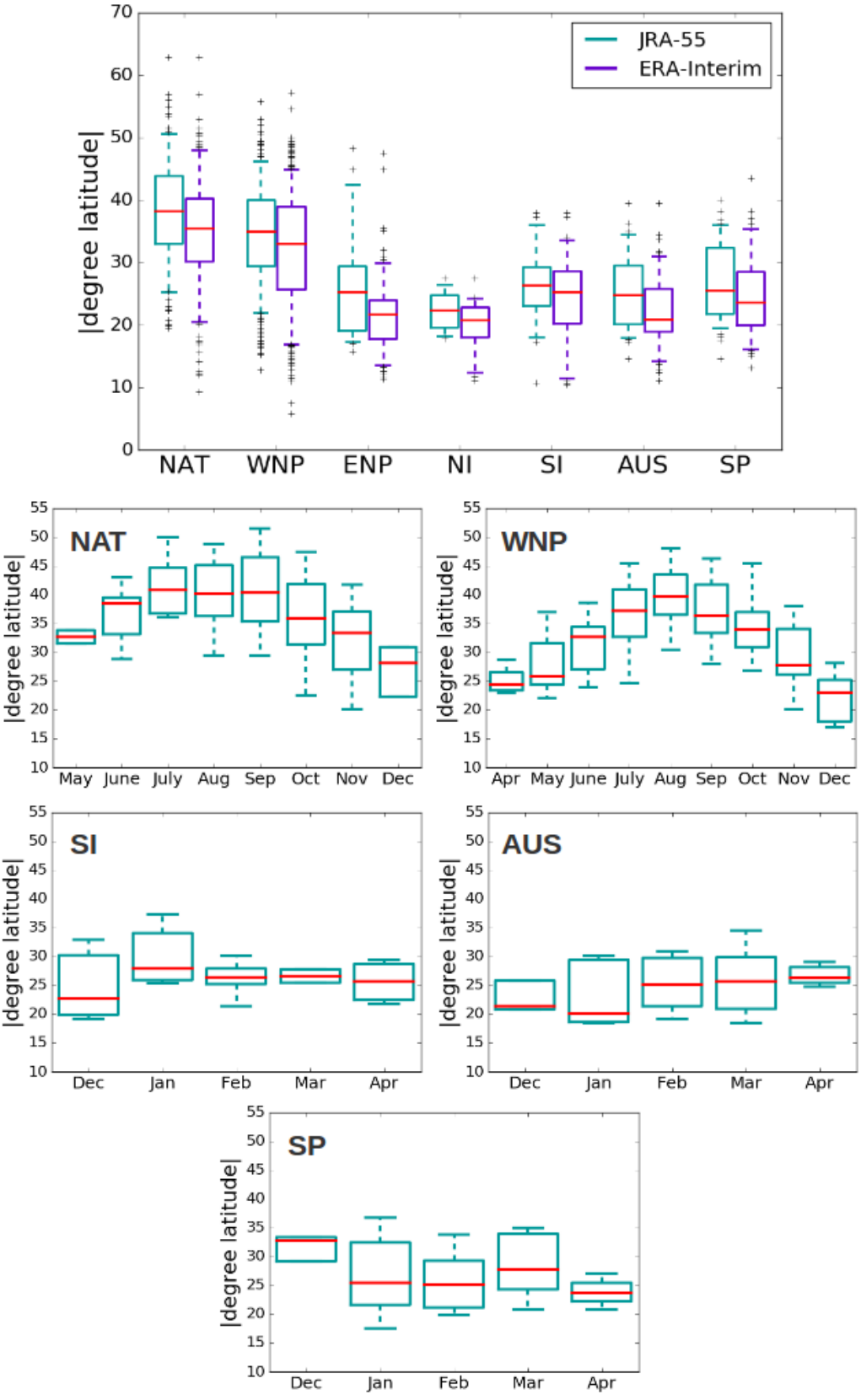
JRA-55
ERA-Interim
|degree latitude|
NAT
WNP
ENP
NI
SI
AUS
SP
May June July Aug Sep Oct Nov Dec
Apr May June July Aug Sep Oct Nov Dec
Dec Jan Feb Mar Apr

FIG. 9. Box plots of the absolute values of the latitudes at which storms complete ET, for all basins and all ETs in 1979-2015 (top; for JRA-55 and ERA-Interim), and decomposition into seasonal cycles for the NAT, WNP, SI, AUS, and the SP (for JRA-55). The box extends from the lower to the upper quartile, with a red line at the median, and the whiskers extend from the 5^{th} to the 95^{th} percentile.

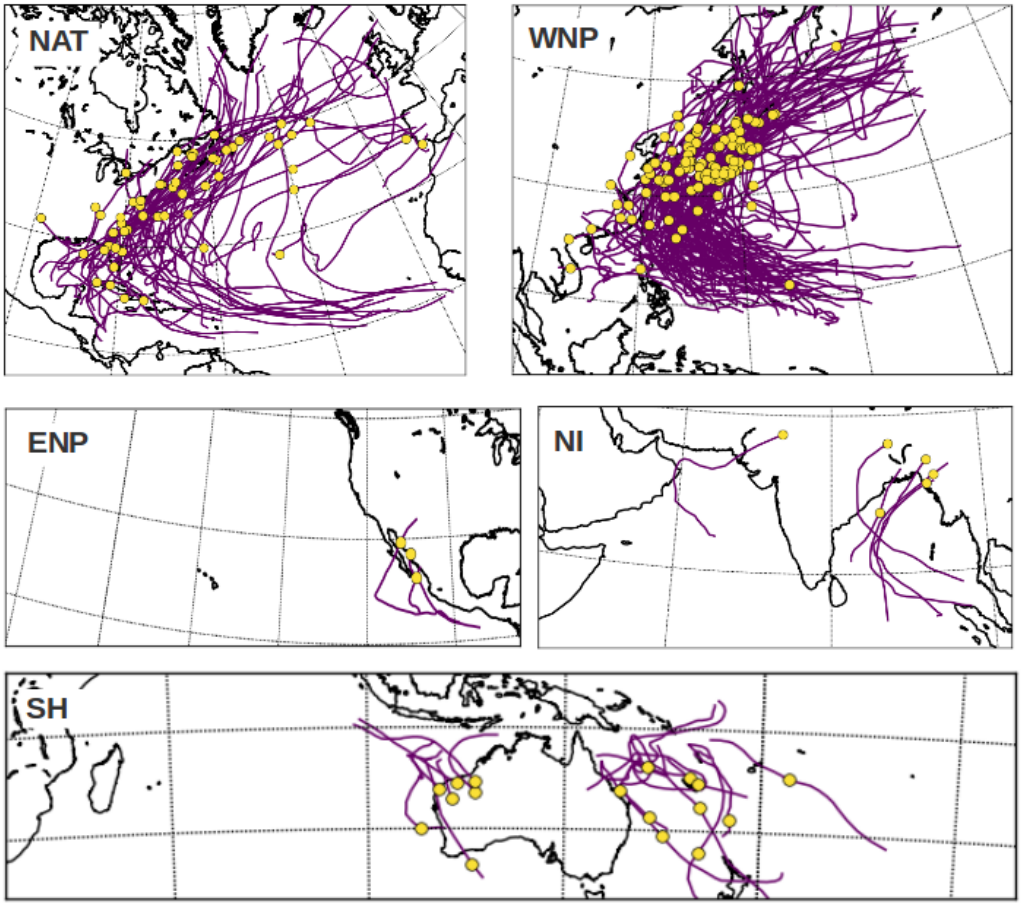

FIG. 10. Tracks of storms that make landfall as transitioning or extratropical systems (according to the JRA-55 classification), for the time period 1979-2015. The yellow dots mark the locations of ET completion.

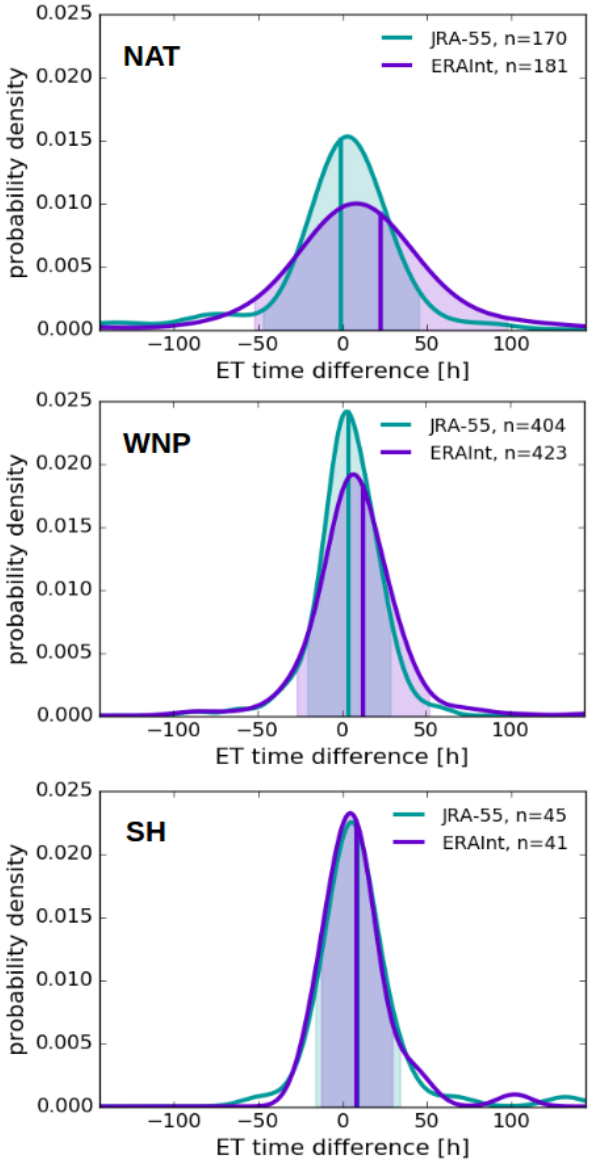

805 FIG. 11. Probability density functions of the differences between the best-track ET times and the ET com-
806 pletion in CPS, based on the ET events from 1979 to 2015 in the NAT and the WNP, and from 2003 to 2015 in
807 the SH. The vertical lines indicate the means of the distributions, and the shaded regions represent values within
808 one standard deviation about the mean. Positive (negative) time differences indicate that the best-track ET time
809 is later than (earlier than) the ET completion in CPS.

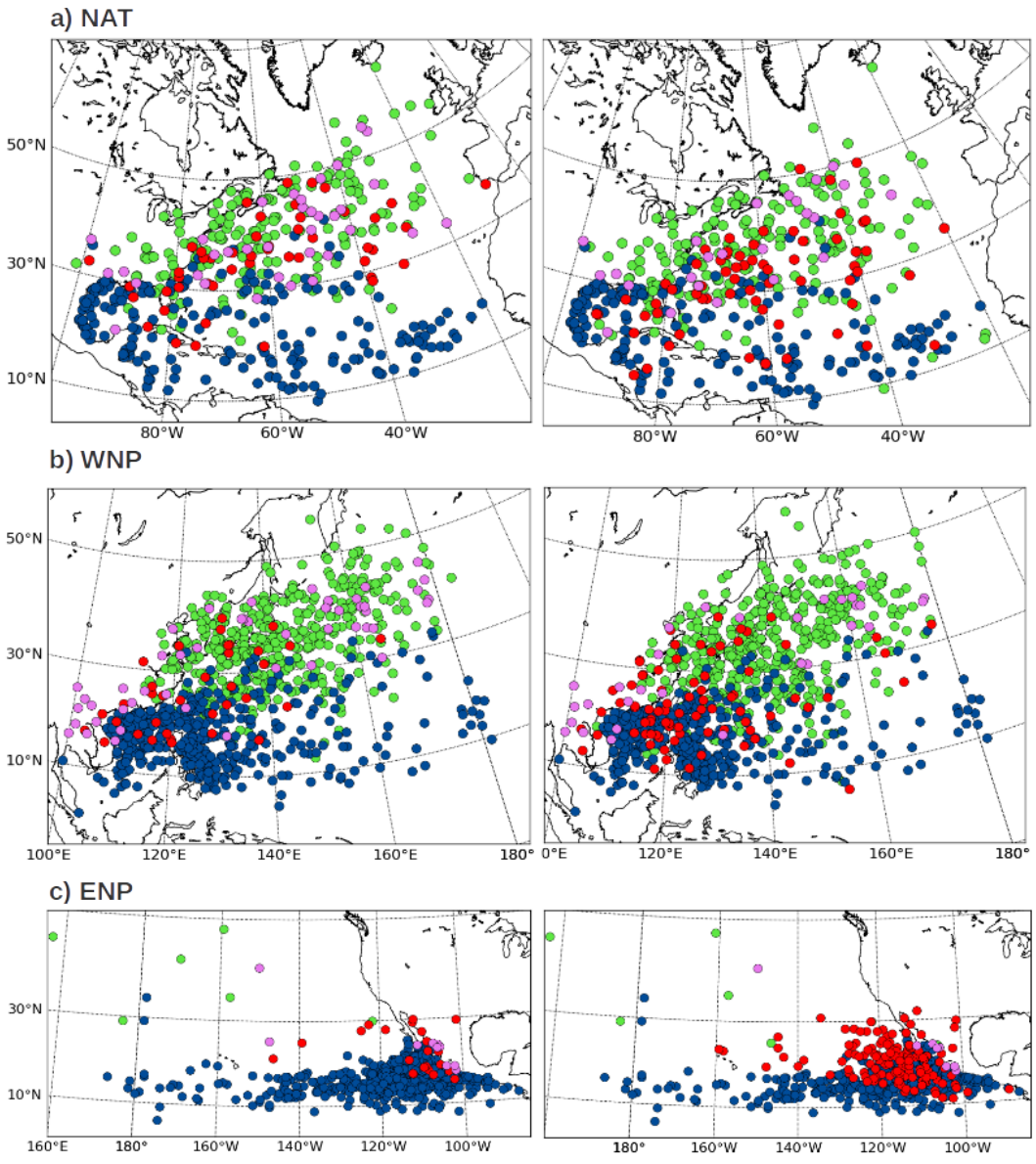

FIG. 12. Comparison of CPS-based ET detection with the best-track labels in the NAT, the WNP, and the ENP, using the JRA-55 (left column) and ERA-Interim (right column) classifications, for the time period 1979-2015. Each dot represents one storm: Green dots mark the position of ET completion for true positive storms (i.e., storms that were classified as ET storms in the CPS-based detection as well as in the best-track labels), red dots denote locations where false positive storms (i.e., storms that were classified as ET storms by the CPS but not by the best-track labels) completed ET, and the ET positions of false negative storms (i.e., storms that were classified as ET storms by the best-track labels but not by the CPS) are shown in magenta – here, the ET position is defined as the location where the storm is for the first time considered extratropical in the best-track data. Finally, the blue dots mark the locations where the true negative storms (which did not undergo ET in either of the two classification methods) acquire their lifetime maximum intensity.

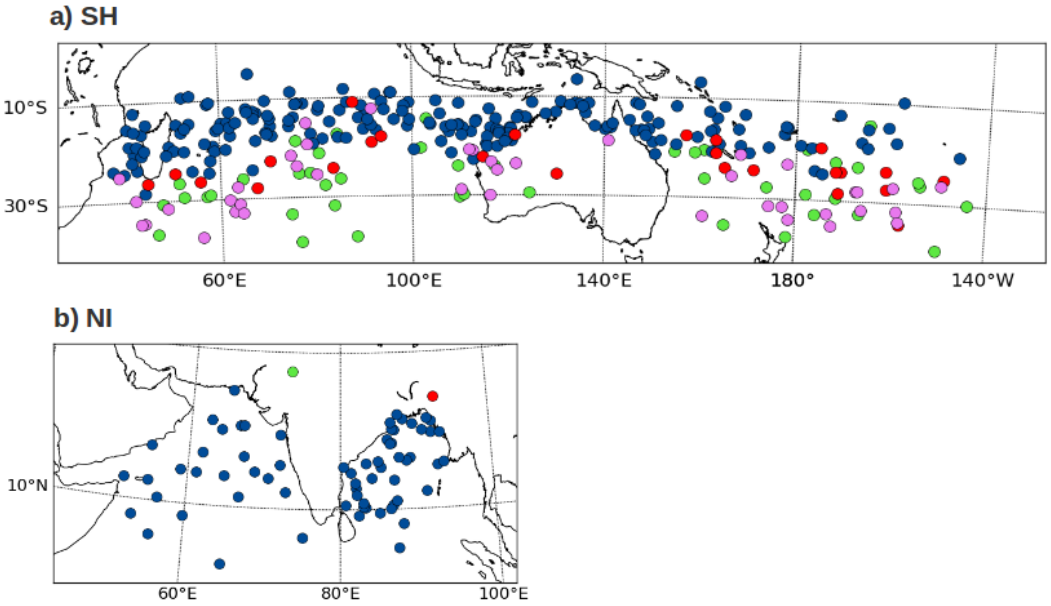

820 FIG. 13. Comparison of CPS-based ET detection (using the JRA-55 classification) with the best-track labels
821 in (a) the SH and (b) the NI, for the time period 2003-2015. The meaning of the dots and colors is the same as
822 in Fig. 12.

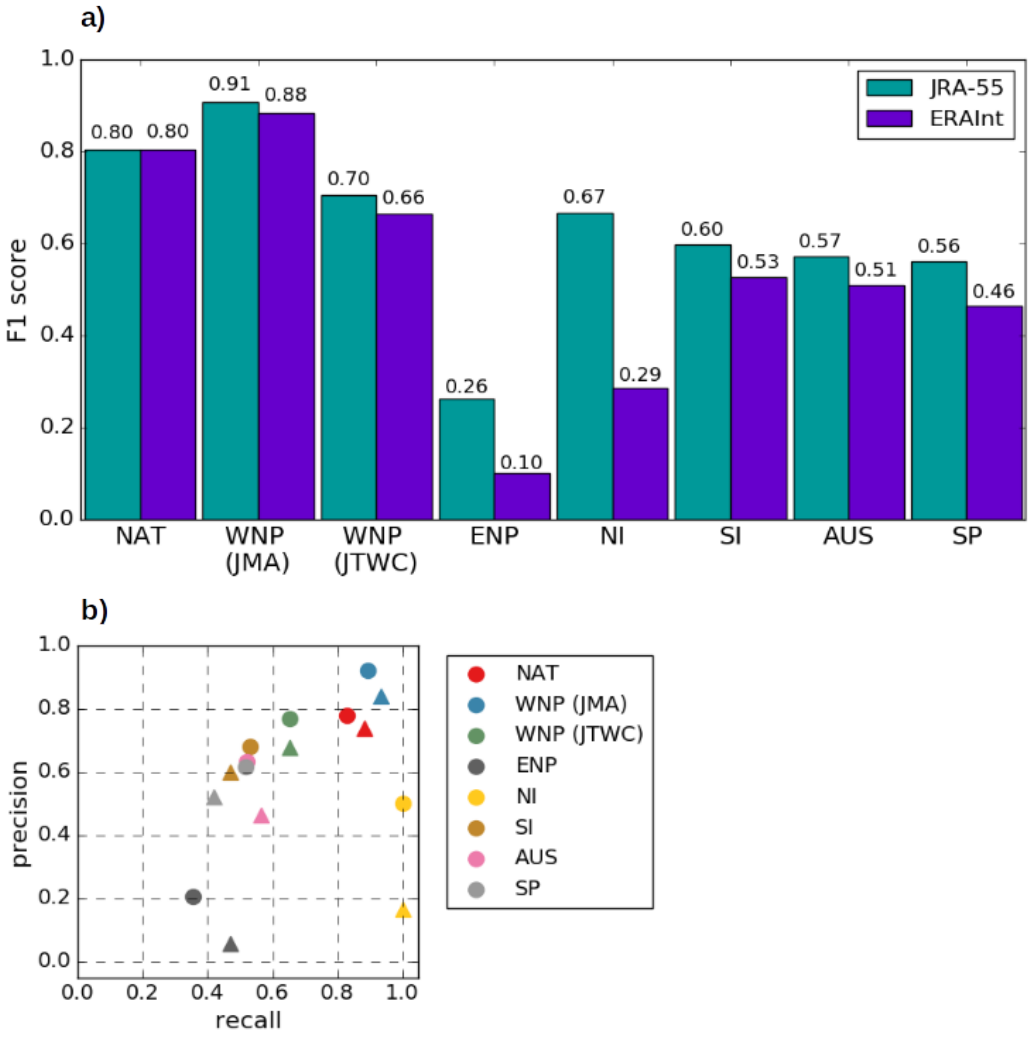

823 FIG. 14. a) F1 scores assessing the performance of the CPS-based ET classification. In the NAT, the WNP
824 (JMA) and the ENP, the F1 scores are based on the period 1979-2015, while the scores for the WNP (JTWC),
825 NI, SI, AUS, and the SP have been calculated based on the period 2003-2015. The results for the WNP are
826 shown for the best-track archives of JMA as well as JTWC. b) Precision and recall associated with the F1 scores
827 in a); scores are marked as circles for JRA-55, and as triangles for ERA-Interim.